

# 1 Impact of Siberian observations on the optimization of 2 surface CO<sub>2</sub> flux

3  
4 **Jinwoong Kim<sup>1\*</sup>, Hyun Mee Kim<sup>1</sup>, Chun-Ho Cho<sup>2</sup>, Kyung-On Boo<sup>2</sup>, Andrew R.  
5 Jacobson<sup>3, 4</sup>, Motoki Sasakawa<sup>5</sup>, Toshinobu Machida<sup>5</sup>, Mikhail Arshinov<sup>6</sup>, and  
6 Nikolay Fedoseev<sup>7</sup>**

7 [1]{Department of Atmospheric Sciences, Yonsei University, Seoul, Republic of Korea}

8 [2]{National Institute of Meteorological Research, Jeju, Republic of Korea}

9 [3]{Earth System Research Laboratory, National Oceanic and Atmospheric Administration,  
10 Boulder, USA}

11 [4]{Cooperative Institute for Research in Environmental Sciences, University of Colorado,  
12 Boulder, USA}

13 [5]{Center for Global Environmental Research, National Institute for Environment Studies,  
14 Tsukuba, Japan}

15 [6]{V. E. Zuev Institute of Atmospheric Optics, Russian Academy of Sciences, Tomsk,  
16 Russia}

17 [7]{Melnikov Permafrost Institute, Russian Academy of Sciences, Yakutsk, Russia}

18 Correspondence to: Hyun Mee Kim (khm@yonsei.ac.kr)

## 19 20 **Abstract**

21 To investigate the effect of additional CO<sub>2</sub> observations in the Siberia region on the Asian and  
22 global surface CO<sub>2</sub> flux analyses, two experiments using different observation dataset were  
23 performed for 2000-2009. One experiment was conducted using a data set that includes  
24 additional observations of Siberian tower measurements (Japan-Russia Siberian Tall Tower  
25 Inland Observation Network: JR-STATION), and the other experiment was conducted using a  
26 data set without the above additional observations. The results show that the global balance of  
27 the sources and sinks of surface CO<sub>2</sub> fluxes was maintained for both experiments with and  
28 without the additional observations. While the magnitude of the optimized surface CO<sub>2</sub> flux

1 uptake and flux uncertainty in Siberia decreased from  $-1.17 \pm 0.93 \text{ Pg C yr}^{-1}$  to  $-0.77 \pm 0.70 \text{ Pg}$   
2  $\text{C yr}^{-1}$ , the magnitude of the optimized surface  $\text{CO}_2$  flux uptake in the other regions (e.g.,  
3 Europe) of the Northern Hemisphere (NH) land increased for the experiment with the  
4 additional observations, which affect the longitudinal distribution of the total NH sinks. This  
5 change was mostly caused by changes in the magnitudes of surface  $\text{CO}_2$  flux in June and July.  
6 The observation impact measured by uncertainty reduction and self-sensitivity tests shows  
7 that additional observations provide useful information on the estimated surface  $\text{CO}_2$  flux.  
8 The average uncertainty reduction of the Conifer Forest of EB is 29.1% and the average self-  
9 sensitivities at the JR-STATION sites are approximately 60% larger than those at the towers  
10 in North America. It is expected that the Siberian observations play an important role in  
11 estimating surface  $\text{CO}_2$  flux in the NH land (e.g., Siberia and Europe) in the future.

12

## 13 **1 Introduction**

14 The terrestrial ecosystem in the Northern Hemisphere (NH) plays an important role in the  
15 global carbon balance (Hayes et al., 2011; Le Quéré et al., 2015). Especially, Siberia is  
16 considered to be the one of the largest  $\text{CO}_2$  uptake regions and reservoirs due to its forest area  
17 (Schulze et al., 1999; Houghton et al., 2007; Tarnocai et al., 2009; Kurganova et al., 2010;  
18 Schepaschenko et al., 2011) and its dynamics and interactions with the climate have global  
19 significance (Quegan et al., 2011). Therefore, it is important to accurately estimate the surface  
20  $\text{CO}_2$  fluxes in this region. For instance, Dolman et al. (2012) estimated terrestrial carbon  
21 budget of Russia, Ukraine, Belarus, and Kazakhstan using inventory-based, eddy covariance,  
22 and inversion methods and showed that the carbon budgets produced by three methods agree  
23 within their uncertainty bounds.

24 To estimate the surface  $\text{CO}_2$  flux, atmospheric  $\text{CO}_2$  inversion studies are conducted using  
25 atmospheric transport models and atmospheric  $\text{CO}_2$  observations (Gurney et al., 2002; Peylin  
26 et al., 2013). However, prior emission, measurement error of observation, observation  
27 operator including model transport, and representative error affect the uncertainty of  
28 atmospheric inversion results (Engelen et al., 2002; Berchet et al., 2015a). Along these factors,  
29 large uncertainties remain in the estimated surface  $\text{CO}_2$  fluxes due to the sparseness of current  
30 surface  $\text{CO}_2$  measurements assimilated by inverse models (Peters et al., 2010; Bruhwiler et al.,  
31 2011). Peylin et al. (2013) performed an intercomparison study of estimated surface  $\text{CO}_2$

1 fluxes from 11 different inversion systems. The results showed that the estimated surface CO<sub>2</sub>  
2 flux uptake in the NH, where the atmospheric CO<sub>2</sub> network is dense, is similar across the  
3 inversion systems; meanwhile, the established flux is noticeably different across the inversion  
4 systems for the tropics and SH, where the atmospheric CO<sub>2</sub> network is sparse.

5 Regionally, however, the longitudinal breakdown of all the NH sinks appears to be much  
6 more variable than the total flux itself. Therefore, additional observations in a sparse CO<sub>2</sub>  
7 observation network region are necessary to reduce uncertainty in estimating the surface CO<sub>2</sub>  
8 flux. Maksyutov et al. (2003) showed that additional observations in the Asia region show the  
9 largest effect and reduce the uncertainty in the estimated regional CO<sub>2</sub> fluxes for Siberia  
10 during 1992-1996 by time-independent synthesis inversion. Chevallier et al. (2010) also  
11 argued that an extension of the observation network toward Eastern Europe and Siberia is  
12 necessary to reduce uncertainty in estimated fluxes by inversion methods. Despite the  
13 necessity of additional observations in this region, only a few atmospheric CO<sub>2</sub> inversion  
14 studies have been conducted using observations in this region due to the deficiency of  
15 observations (Quegan et al., 2011).

16 Meanwhile, Reuter et al. (2014) and Feng et al. (2016) reported that the European terrestrial  
17 CO<sub>2</sub> uptake inferred by the satellite-retrieved dry-air column-average mole fraction of CO<sub>2</sub>  
18 (XCO<sub>2</sub>) is larger than that inferred by a bottom-up inventory approach or inverse modeling  
19 systems using surface-based CO<sub>2</sub> atmospheric concentrations. Though a broad spatial  
20 coverage of XCO<sub>2</sub> from satellite radiance observations provides useful information for  
21 inversion systems in quantifying surface CO<sub>2</sub> fluxes at various scales which is not provided  
22 by ground-based measurements, the current XCO<sub>2</sub> has low accuracy and regional biases of a  
23 few tenths of a ppm, which may hamper the accuracy of estimated surface CO<sub>2</sub> fluxes (Miller  
24 et al., 2007; Chevallier et al., 2007). Therefore, in situ observations determined by surface  
25 measurements are necessary to more accurately estimate the surface CO<sub>2</sub> flux in the inverse  
26 models.

27 To supply additional observations over Siberia to inverse modeling studies, several efforts to  
28 observe the atmospheric CO<sub>2</sub> concentrations in Siberia have been conducted. For example, the  
29 Max Planck Institute (MPI) operates a tower (since April 2009), preceded by aircraft  
30 measurements (from 1998 to 2005 with 12 to 21 day intervals) at Zotino (ZOTTO; 60.75°N,  
31 89.38°E) (Lloyd et al., 2002; Winderlich et al. 2010). In addition, the Airborne Extensive  
32 Regional Observations in Siberia (YAK-AEROSIB) aircraft campaign in 2006 (Paris et al.,

1 2008) and Trans-Siberian Observation Into the Chemistry of the Atmosphere (TROICA)  
2 project (Turnbull et al., 2009) have measured CO<sub>2</sub> and other chemical species. However,  
3 except Zotino that has multi-year measurements, these data collected during specific seasons  
4 or over only a few years do not provide the long-term CO<sub>2</sub> concentration data necessary to be  
5 used as a constraint in the inverse modeling system.

6 The Center for Global Environmental Research (CGER) of the National Institute for  
7 Environmental Studies (NIES) of Japan with the cooperation of the Russian Academy of  
8 Science (RAS) constructed a tower network called the Japan-Russia Siberian Tall Tower  
9 Inland Observation Network (JR-STATION) in 2002 to measure the continuous CO<sub>2</sub> and CH<sub>4</sub>  
10 concentrations (eight towers in central Siberia and one tower in eastern Siberia) (Sasakawa et  
11 al., 2010, 2013). The vertical profile of CO<sub>2</sub> concentrations from the planetary boundary layer  
12 (PBL) to the lower free troposphere is also measured by aircraft at one site of the JR-  
13 STATION sites (Sasakawa et al., 2010, 2013). Saeki et al. (2013) estimated the monthly  
14 surface CO<sub>2</sub> flux for 68 subcontinental regions by using the fixed-lag Kalman smoother and  
15 NIES-TM transport model with JR-STATION data. They reported that the inclusion of  
16 additional Siberian observation data has an impact on the inversion results showing larger  
17 interannual variability over northeastern Europe as well as Siberia, and reduces the  
18 uncertainty of surface CO<sub>2</sub> uptake. Meanwhile, Berchet et al. (2015b) estimated regional CH<sub>4</sub>  
19 fluxes over Siberia in 2010 by using JR-STATION data.

20 CarbonTracker, developed by the National Oceanic and Atmospheric Administration Earth  
21 System Research Laboratory (NOAA ESRL) (Peters et al., 2007), is an atmospheric CO<sub>2</sub>  
22 inverse modeling system that estimates optimized weekly surface CO<sub>2</sub> flux on a 1°×1°  
23 horizontal resolution by using the Ensemble Kalman Filter (EnKF). Since the original  
24 CarbonTracker release (Peters et al 2007), a series of improvements have been made with  
25 subsequent releases. These include increasing the number of sites from which CO<sub>2</sub> data are  
26 assimilated, increasing the resolution of atmospheric transport, improving the simulation of  
27 atmospheric convection in TM5, and the use of multiple first-guess flux models to estimate  
28 sensitivity to priors. These improvements are documented at <http://carbontracker.noaa.gov>.  
29 Several studies have focused on Asia using CarbonTracker (Kim et al., 2012, 2014a, b; Zhang  
30 et al., 2014a, b). Schneising et al. (2011) showed that SCanning Imaging Absorption  
31 spectroMeter for Atmospheric CHartography (SCIAMACHY) retrieval data indicate a  
32 stronger North American boreal forest uptake and weaker Russian boreal forest uptake

1 compared to CarbonTracker within their uncertainties. On the other hand, Zhang et al.  
2 (2014b) estimated surface CO<sub>2</sub> fluxes in Asia by assimilating CONTRAIL (Machida et al.,  
3 2008) aircraft CO<sub>2</sub> measurements into the CarbonTracker framework. The CONTRAIL  
4 measurements include ascending/descending vertical profiles and cruise data below  
5 tropopause. The results show that surface CO<sub>2</sub> uptake over the Eurasian Boreal (EB) region  
6 slightly increases from -0.96 Pg C yr<sup>-1</sup> to -1.02 Pg C yr<sup>-1</sup> for the period 2006-2010 when  
7 aircraft CO<sub>2</sub> measurements were assimilated. However, the surface measurements data over  
8 the EB region are still not used in the study by Zhang et al. (2014b). Using an influence  
9 matrix calculation, Kim et al. (2014b) showed that comprehensive coverage of additional  
10 observations in an observation sparse region, e.g., Siberia, is necessary to estimate the surface  
11 CO<sub>2</sub> flux in these areas as accurately as that obtained for North America in the CarbonTracker  
12 framework.

13 In this study, the impact of additional Siberian observations on the optimized surface CO<sub>2</sub>  
14 flux over the globe and Asian region within CarbonTracker (The version of CarbonTracker  
15 used in this study is based on the CarbonTracker 2010 release) are investigated by comparing  
16 the results of estimated surface CO<sub>2</sub> fluxes from two experiments with and without Siberian  
17 observations. Section 2 presents the methodology including a priori flux data, atmospheric  
18 CO<sub>2</sub> observations, and experimental framework. Section 3 presents the results, and Section 4  
19 provides a summary and conclusions.

20

## 21 **2 Methodology**

### 22 **2.1 Inversion method**

23 CarbonTracker is an inverse modeling system developed by Peters et al. (2007). Optimized  
24 surface CO<sub>2</sub> fluxes with a 1°×1° horizontal resolution are calculated as follows:

$$25 \quad F(x, y, t) = \lambda_r \cdot F_{bio}(x, y, t) + \lambda_r \cdot F_{ocn}(x, y, t) + F_{ff}(x, y, t) + F_{fire}(x, y, t), \quad (1)$$

26 where  $F_{bio}(x, y, t)$ ,  $F_{ocn}(x, y, t)$ ,  $F_{ff}(x, y, t)$ , and  $F_{fire}(x, y, t)$  are a priori emissions from the  
27 biosphere, the ocean, fossil fuel, and fires.  $\lambda_r$  is the scaling factor to be optimized in the data  
28 assimilation process, corresponding to 156 regions around the globe (126 land and 30 ocean  
29 regions). In the land, the ecoregions are defined as the combination of 11 land region of  
30 Transcom regions (Gurney et al., 2002) with 19 land-surface characterization based on Olson

1 et al. (1992). Inappropriate combinations of TransCom regions and Olson types are excluded.  
 2 In the ocean, 30 ocean regions are defined following Jacobson et al. (2007). The scaling factor  
 3 spans 5 weeks with 1 week resolution. Several previous studies for CarbonTracker (e.g.,  
 4 Peters et al., 2007; 2010, Kim et al., 2012, 2014a, b; Zhang et al., 2014a, b; van der Laan-  
 5 Luijkx et al., 2015) showed that 5 weeks of lag and 1-week time resolution are appropriate for  
 6 optimizing the surface CO<sub>2</sub> fluxes. In each assimilation cycle (i.e., analysis step), the entire  
 7 scaling factor for 5 weeks is updated by 1 week observations measured most recent week by a  
 8 time stepping approach. The smoother window moves forward by 1 week at each assimilation  
 9 cycle. After 5 assimilation cycles, the first part of the scaling factor analyzed by 5 weeks  
 10 observations is regarded as the optimized scaling factor. The more detailed information of the  
 11 assimilation process can be found in Kim et al. (2014b).

12 The ensemble Kalman filter (EnKF) data assimilation method used in CarbonTracker is the  
 13 ensemble square root filter (EnSRF) suggested by Whitaker and Hamill (2002). The analysis  
 14 equation for data assimilation is expressed as

$$15 \quad \mathbf{x}^a = \mathbf{K}\mathbf{y}^o + (\mathbf{I}_n - \mathbf{K}\mathbf{H})\mathbf{x}^b, \quad (2)$$

16 where  $\mathbf{x}^a$  is the n-dimensional analysis (posterior) state vector ;  $\mathbf{y}^o$  is the p-dimensional  
 17 observation vector (atmospheric CO<sub>2</sub> observations);  $\mathbf{K}$  is the  $n \times p$  dimensional Kalman gain;  
 18  $\mathbf{I}_n$  is the identity matrix;  $\mathbf{H}$  is the linearized observation operator, which transforms the  
 19 information in the model space to the information in the observation space; and  $\mathbf{x}^b$  is the  
 20 background state vector. In CarbonTracker, the state vector corresponds to the scaling factor.  
 21 The Kalman gain  $\mathbf{K}$  is defined as

$$22 \quad \mathbf{K} = (\mathbf{P}^b \mathbf{H}^T) (\mathbf{H} \mathbf{P}^b \mathbf{H}^T + \mathbf{R})^{-1}, \quad (3)$$

23 where  $\mathbf{P}^b$  is the background error covariance;  $\mathbf{R}$  is the observation error covariance or model  
 24 data mismatch, which is predefined at each observation site.  $\mathbf{P}^b \mathbf{H}^T$  and  $\mathbf{H} \mathbf{P}^b \mathbf{H}^T$  in Eq. (3) can  
 25 be calculated as

$$26 \quad \mathbf{P}^b \mathbf{H}^T \approx \frac{1}{m-1} (\mathbf{x}'_1, \mathbf{x}'_2, \dots, \mathbf{x}'_m) \cdot (\mathbf{H}\mathbf{x}'_1, \mathbf{H}\mathbf{x}'_2, \dots, \mathbf{H}\mathbf{x}'_m)^T, \quad (4)$$

$$27 \quad \mathbf{H} \mathbf{P}^b \mathbf{H}^T \approx \frac{1}{m-1} (\mathbf{H}\mathbf{x}'_1, \mathbf{H}\mathbf{x}'_2, \dots, \mathbf{H}\mathbf{x}'_m) \cdot (\mathbf{H}\mathbf{x}'_1, \mathbf{H}\mathbf{x}'_2, \dots, \mathbf{H}\mathbf{x}'_m)^T, \quad (5)$$

1 where  $m$  is the number of ensembles and  $'$  denotes the perturbation of ensemble mean.

2 The sampling error caused by the limited ensemble size may degrade the analysis accuracy.

3 To reduce the impact of sampling error in the EnKF, the covariance localization method is

4 used (Houtekamer and Mitchell, 2001). The localization is not applied to Marine Boundary

5 Layer (MBL) sites (e.g. observation sites in Antarctica), because the MBL sites are

6 considered as including information on large footprints of flux signals (Peters et al., 2007).

7 The physical distance between the scaling factors cannot be defined. Therefore, localization is

8 performed based on the linear correlation coefficient between the ensemble of the scaling

9 factor and the ensemble of the model CO<sub>2</sub> concentration (Peters et al., 2007). Statistical

10 significance test is performed on the linear correlation coefficient with a cut-off at a 95%

11 significance in a student's T-test. Then the components of Kalman gain with an insignificant

12 statistical value are set to zero.

13 After one analysis step is completed, the new mean scaling factor that serves as the

14 background scaling factor for next analysis cycle is predicted as

$$15 \quad \lambda_t^b = \frac{(\lambda_{t-2}^a + \lambda_{t-1}^a + 1)}{3}, \quad (6)$$

16 where  $\lambda_t^b$  is a prior mean scaling factor of the current analysis cycle,  $\lambda_{t-2}^a$  and  $\lambda_{t-1}^a$  are

17 posterior mean scaling factors of previous cycles. Eq. (6) propagates information from one

18 step to the next step (Peters et al., 2007).

19 The detailed algorithm of inversion method used in this study can be found in Peters et al.

20 (2007) and Kim et al. (2014a).

## 21 **2.2 A priori flux data**

22 Four types of a priori and imposed CO<sub>2</sub> fluxes used in this study are as follows: (1) First guess

23 biosphere flux from the Carnegie–Ames–Stanford Approach Global Fire Emissions Database

24 (CASA GFED) version 3.1 (van der Werf et al., 2010). The 3 hour interval Net Ecosystem

25 Exchange (NEE) is calculated from monthly mean Net Primary Production (NPP) and

1 ecosystem respiration (RE) by using a simple temperature  $Q_{10}^1$  relationship and a linear  
2 scaling of photosynthesis with solar radiation (Olsen and Randerson, 2004); (2) the prior  
3 ocean flux from air-sea partial pressure differences based on Jacobson et al. (2007). Short-  
4 term flux variability is derived from the atmospheric model wind speeds via the gas transfer  
5 coefficient; (3) biomass burning emissions obtained from GFED v3.1 (van der Werf et al.,  
6 2010); (4) the prescribed fossil fuel emission from the Carbon Dioxide Information and  
7 Analysis Center (CDIAC, Boden et al., 2010) and the Emission Database for Global  
8 Atmospheric Research (EDGAR, European Commission, 2009) databases. The annual global  
9 total fossil fuel emissions are based on CDIAC. Fluxes at  $1^\circ \times 1^\circ$  resolution are spatially  
10 distributed according to the EDGAR inventories.

### 11 **2.3 Atmospheric CO<sub>2</sub> observations**

12 Atmospheric CO<sub>2</sub> mole fraction observations measured at surface observation sites are used in  
13 this study. Figure 1 shows the observation network and Table 1 presents observation site  
14 information for the Asian and European regions. Three sets of atmospheric CO<sub>2</sub> observations  
15 data are assimilated: (1) surface CO<sub>2</sub> observations distributed by the NOAA ESRL  
16 (observation sites operated by NOAA, Environment Canada (EC), the Australian  
17 Commonwealth Scientific and Industrial Research Organization (CSIRO), the National  
18 Center for Atmospheric Research (NCAR), and Lawrence Berkeley National Laboratory  
19 (LBNL)) (observation data is available at [http://www.esrl.noaa.gov/gmd/ccgg/obspack/  
20 data.php](http://www.esrl.noaa.gov/gmd/ccgg/obspack/data.php); Masarie et al., 2014); (2) World Data Centre for Greenhouse Gases (WDCGG,  
21 <http://ds.data.jma.go.jp/wdcgg/>); (3) JR-STATION observation data over Siberia operated by  
22 CGER/NIES (Sasakawa et al., 2010, 2013). The JR-STATION sites consist of nine towers  
23 (eight towers in west Siberia and one tower in east Siberia). Atmospheric air was sampled at  
24 four levels on the BRZ tower and at two levels on the other eight towers. At the BRZ  
25 (Berezorechka) site in west Siberia, both tower and aircraft measurements are sampled. The  
26 light aircraft at BRZ site measures the vertical profiles of CO<sub>2</sub> from the PBL to the lower free  
27 troposphere and these vertical profiles are used as independent observations for verification.

---

<sup>1</sup> It is calculated as  $Q_{10}(t) = 1.5^{((T_{2m} - T_0)/10.0)}$ , where  $t$  is time,  $T_{2m}$  is temperature (K) at 2 m, and  $T_0$  is 273.15 K.



1 Sampled CO<sub>2</sub> data were calibrated against the NIES 09 CO<sub>2</sub> scale which are lower than the  
2 WMO-X2007 CO<sub>2</sub> scale by 0.07 ppm at around 360 ppm and consistent in the range between  
3 380 and 400 ppm (Machida et al., 2011). Detailed description of JR-STATION sites can be  
4 found in Sasakawa et al. (2010, 2013). Daytime averaged CO<sub>2</sub> concentrations (1200-1600  
5 LST, representing the time when active vertical mixing occurred in the PBL) for each day  
6 from the time series at the highest level of tower measurements are used in the data  
7 assimilation.

8 In CarbonTracker, model data mismatch (MDM,  $\mathbf{R}$  in Eq. (7)) is assigned by site categories.  
9 The location of each observation site is represented in Fig. 1. The assigned MDM requires  
10 innovation  $\chi^2$  statistics in Eq. (7) become close to one at each observation site (Peters et al.  
11 2007).

$$12 \quad \chi^2 = \frac{(\mathbf{y}^o - \mathbf{H}\mathbf{x}^b)^2}{\mathbf{H}\mathbf{P}^b\mathbf{H}^T + \mathbf{R}}, \quad (7)$$

13 where  $\mathbf{y}^o - \mathbf{H}\mathbf{x}^b$  represent innovation. The site categories and MDM values are assigned the  
14 same value as in previous studies (Peters et al., 2007; Kim et al. 2014b; Zhang et al., 2014b):  
15 marine boundary layer (0.75 ppm), continental sites (2.5 ppm), mixed land/ocean and  
16 mountain sites (1.5 ppm), continuous sites (3.0 ppm), and difficult sites (7.5 ppm).  
17 Continuous site category is generally used for observations measured continuously. For the  
18 JR-STATION sites that have continuous tower measurements, the MDM is set to 3 ppm,  
19 which is the same as tower measurements in North America.

## 20 **2.4 Experimental framework**

21 Two experiments with different set of observations are conducted in this study: one  
22 experiment, the CNTL experiment, is conducted by using set of observations without  
23 observations in the Siberia region (black color observation sites represented in Fig. 1); the  
24 other experiment, the JR experiment, is conducted by using all available observations  
25 including the Siberia data (all observation sites represented in Fig. 1). The TM5 model (Krol  
26 et al., 2005) which calculates four-dimensional CO<sub>2</sub> concentration field runs at global 3°×2°  
27 horizontal resolution and a nesting domain centered in Asia with 1°×1° horizontal resolution.  
28 The nesting domain is shown in Fig. 1. Meteorological variables for running the TM5  
29 transport model are from the European Centre for Medium-Range Weather Forecasts  
30 (ECMWF) forecast model output. The experimental period is from 1 January 2000 to 31

1 December 2009. The observation data commonly used for CNTL and JR experiments exist  
2 from 2000, but the additional Siberia data for the JR experiment exist from 2002. The number  
3 of ensembles is 150, and the scaling factor includes 5 weeks of lag, as in previous studies  
4 (Peters et al., 2007, 2010; Peylin et al., 2013; Kim et al., 2012, 2014a b; Zhang et al., 2014a,  
5 b).

6

## 7 **3 Results**

### 8 **3.1 Characteristics of carbon fluxes**

9 In this section, optimized surface CO<sub>2</sub> fluxes inferred from the two experiments are examined.  
10 The optimized surface CO<sub>2</sub> flux in 2000 and 2001 is excluded from this analysis because  
11 2000 is considered a spin-up year similar to previous studies using CarbonTracker, and JR-  
12 STATION data are used since 2002. Only the biosphere and ocean fluxes are presented here  
13 because fires (biomass burning) and fossil fuel emissions are not optimized in CarbonTracker.

14 Figure 2 presents the spatial distribution of the averaged prior and optimized biosphere and  
15 ocean fluxes of the two experiments and the difference between the CNTL and JR  
16 experiments from 2002 to 2009. The optimized biosphere flux uptakes of the CNTL and JR  
17 experiments are globally 1.60 ~ 1.61 Pg C yr<sup>-1</sup> greater than the prior flux uptakes (Figs. 2a, c,  
18 d, Table 2). The difference in fluxes between the prior and JR experiment is large in EB (Figs.  
19 2a, d) although smaller than that between the prior and CNTL experiment (Figs. 2a, c). The  
20 differences in fluxes between the CNTL and JR experiments are distinctive in EB (Siberia)  
21 where the new additional observations are assimilated (Fig. 2b). The magnitude of surface  
22 CO<sub>2</sub> uptakes decreases in that region by assimilating JR-STATION observation data. On the  
23 contrary, the average surface CO<sub>2</sub> uptakes in other regions, such as North America, Europe,  
24 the western North Pacific Ocean, and the Atlantic Ocean, increase by assimilating JR-  
25 STATION observation data.

26 The difference in the optimized CO<sub>2</sub> flux between the two experiments is analyzed. Table 2  
27 presents prior and optimized fluxes with their uncertainties for global total, global land, global  
28 ocean, NH total, Tropics total, Southern Hemisphere total, and TransCom regions in the NH.  
29 Flux uncertainties are calculated from the ensembles of prior and optimized surface fluxes  
30 assuming Gaussian errors, following previous method used in Peters et al. (2007, 2010). The  
31 global total biogenic and oceanic optimized CO<sub>2</sub> fluxes are similar for each experiment at -

1 5.54±1.85 Pg C yr<sup>-1</sup> (CNTL experiment) and -5.55±1.72 Pg C yr<sup>-1</sup> (JR experiment), compared  
2 with the global prior flux of -3.94±2.24 Pg C yr<sup>-1</sup>. The global land sink in the CNTL  
3 experiment is larger by 0.07 Pg C yr<sup>-1</sup> than that of the JR experiment, and the global ocean  
4 sink in the CNTL experiment is smaller by 0.08 Pg C yr<sup>-1</sup> than that of the JR experiment. The  
5 additional observations do not make any discrepancy between the two experiments with  
6 respect to the global total sink, and they indicate only a small difference in the land-ocean  
7 CO<sub>2</sub> flux partitioning. The estimated CO<sub>2</sub> flux uncertainty in the land region from the JR  
8 experiment is smaller than that of the CNTL experiment because new observations provide  
9 additional constraints on the optimized CO<sub>2</sub> flux. For specific regions in the NH, a large  
10 difference of optimized surface CO<sub>2</sub> flux is observed in the EB. The largest increment  
11 between a priori and CNTL is shown in EB with the least in situ observations as shown in Fig.  
12 1. The other regions show smaller increment with more ‘local’ observations available. The  
13 surface CO<sub>2</sub> uptakes in the EB of the CNTL experiment is -1.17±0.93 Pg C yr<sup>-1</sup> and that of the  
14 JR experiment is -0.77±0.70 Pg C yr<sup>-1</sup>, respectively. The uncertainty of the optimized surface  
15 CO<sub>2</sub> uptake in the EB in the JR experiment is expectedly reduced by assimilating additional  
16 observations. In contrast, the surface CO<sub>2</sub> uptake increases in other regions of the NH.

17 Figure 3 presents the spatial distribution of the optimized biosphere fluxes difference between  
18 the CNTL and JR experiments from 2002 to 2009. The difference of optimized surface CO<sub>2</sub>  
19 flux is calculated as in Fig. 2b. The largest difference of optimized surface CO<sub>2</sub> fluxes  
20 between the two experiments occurs in Siberia. The uptake of optimized surface CO<sub>2</sub> flux in  
21 this region is reduced in JR for all years except 2003. In 2003, extreme drought occurred in  
22 the northern mid-latitudes (Knorr et al., 2007) and Europe (Ciais et al., 2005), which resulted  
23 in increased NEE (i.e. reduced uptake of CO<sub>2</sub>) in EB in the CNTL experiment. The uptake of  
24 optimized surface CO<sub>2</sub> fluxes in Siberia in 2003 is reduced in the CNTL experiment due to  
25 the remote effect of drought in Europe. Despite the number of JR-STATION data used in the  
26 optimization in 2003 being relatively smaller than that in the later experiment period, new  
27 observations in the JR experiment provide information on the increased uptake of optimized  
28 surface CO<sub>2</sub> fluxes in 2003 in Siberia (Fig. 3b).

29 Optimized surface CO<sub>2</sub> fluxes averaged from 2002 to 2009 for each ecoregion in the NH are  
30 shown in Table 3. In the Siberia (EB), optimized surface CO<sub>2</sub> uptake from the JR experiment  
31 is smaller (larger) than that of the CNTL experiment in the Conifer Forest and Northern Taiga  
32 (in other ecoregions). In the Eurasian Temperate (ET), Europe, North American Boreal

1 (NAB), and North American Temperate (NAT) regions, the optimized surface CO<sub>2</sub> uptakes  
2 from the JR experiment are larger than those of the CNTL experiment in most ecoregions.

3 Figure 4 shows the time series of annual and average prior and optimized surface CO<sub>2</sub> fluxes  
4 over global total, global land, and global ocean. For global total, the magnitude of optimized  
5 fluxes are much greater than that of prior fluxes due to the greater uptake of optimized fluxes  
6 than that of prior fluxes over global land (Figs. 4a and b). In contrast, the magnitude of  
7 optimized fluxes over global ocean is slightly weaker than that of prior fluxes (Fig. 4c). As  
8 shown in Table 2, the differences between annual and average optimized surface CO<sub>2</sub> fluxes  
9 over the globe are small and the average is almost the same for the two experiments (Fig. 4a)  
10 with a similar trend of  $-0.33 \text{ Pg C yr}^{-2}$  and  $-0.35 \text{ Pg C yr}^{-2}$  in CNTL and JR experiment  
11 respectively, and the differences in global land and ocean are also small (Figs. 4b, c) with a  
12 similar trend of  $-0.22 \text{ Pg C yr}^{-2}$  in global land of both CNTL and JR experiment and  $-0.11 \text{ Pg}$   
13  $\text{C yr}^{-2}$  and  $-0.13 \text{ Pg C yr}^{-2}$  in global ocean of CNTL and JR experiment respectively. The  
14 optimized surface CO<sub>2</sub> fluxes from each experiment show similar interannual variability,  
15 which implies that the additional Siberian observations do not affect the interannual  
16 variability of global surface CO<sub>2</sub> uptakes.

17 Figure 5 is the same as Fig. 4 but covers land regions in the NH. Although the optimized  
18 surface CO<sub>2</sub> fluxes over global total are similar, those over each TransCom region are  
19 different in each experiment. The optimized fluxes over each region show greater annual  
20 uptake relative to the prior fluxes in both experiment. The difference between the two  
21 experiments is largest in the EB as expected (Fig. 5a). The JR experiment exhibits a weaker  
22 surface CO<sub>2</sub> uptake in the EB than does the CNTL experiment except for 2003 as shown in  
23 Fig. 3b, whereas the JR experiment exhibits a greater surface CO<sub>2</sub> uptake in the other regions,  
24 especially over Europe in 2008 and 2009, than the CNTL experiment (Figs. 5b, c, d, and e). It  
25 is driven by the increase of CO<sub>2</sub> uptake in Eastern Europe (Figs. 3g and h). Because most of  
26 JR-STATION sites are located in the western part of Siberia (Fig. 1), the optimized surface  
27 CO<sub>2</sub> fluxes over Eastern Europe could be affected by JR-STATION observations. The trend  
28 of EB in CNTL experiment is  $-0.06 \text{ Pg C yr}^{-2}$ , whereas that in JR experiment is  $0.02 \text{ Pg C yr}^{-2}$   
29 due to the reduced uptake of CO<sub>2</sub> in JR experiment since 2005 (Fig 5a). As a result, the trends  
30 of the surface CO<sub>2</sub> uptake of EB and Europe in two experiments show opposite signs. In  
31 contrast, the surface CO<sub>2</sub> uptake trends of other land regions in NH are similar between the  
32 two experiments.

1 Figure 6 shows monthly prior and optimized surface CO<sub>2</sub> fluxes averaged from 2002 to 2009  
2 with their uncertainties from both experiments. In general, optimized fluxes in both  
3 experiments show greater uptake in boreal summer and weaker uptake in other seasons  
4 compared to the prior fluxes, which results in greater annual CO<sub>2</sub> uptake of optimized fluxes  
5 than prior fluxes as shown in Fig. 5. The largest difference in surface CO<sub>2</sub> flux between the  
6 two experiments occurs in June and July, which represent the active season of the terrestrial  
7 ecosystem with a large surface CO<sub>2</sub> flux uncertainty. The JR experiment exhibits a weaker  
8 surface CO<sub>2</sub> summer uptake in the EB (Fig. 6a) and slightly greater uptake in the other  
9 regions (Figs. 6b, c, d, and e). These additional JR-STATION data provides information on  
10 the surface CO<sub>2</sub> uptake by vegetation activities in the NH summer.

### 11 **3.2 Comparison with observations**

12 Table 4 presents the average bias of the model CO<sub>2</sub> concentrations calculated by the  
13 background and optimized fluxes of the two experiments at each observation site located in  
14 Asia and Europe from 2002 to 2009. The bias is calculated by subtracting the observed CO<sub>2</sub>  
15 concentrations from the model CO<sub>2</sub> concentrations. Biases of the JR experiment are smaller  
16 than those of the CNTL experiment at the JR-STATION sites, which indicates that the  
17 optimized surface CO<sub>2</sub> flux of the JR experiment is more consistent with the observed CO<sub>2</sub>  
18 concentrations than that in the CNTL experiment. The negative bias at five JR-STATION  
19 sites (DEM, IGR, KRZ, NOY, and YAK) located in the forest area of the EB is reduced  
20 compared with those of the CNTL experiment, which indicates that the optimized surface  
21 CO<sub>2</sub> uptake of the CNTL experiment is overestimated with respect to CO<sub>2</sub> concentration  
22 observations in Siberia. Otherwise, the reduced surface CO<sub>2</sub> uptake of the JR experiment  
23 exhibits more consistent model CO<sub>2</sub> concentrations in this region. In addition to the average  
24 bias for the entire period, the time series of monthly averaged bias of the model CO<sub>2</sub>  
25 concentration from the observed CO<sub>2</sub> concentration at JR-STATION sites shows that the JR  
26 experiment consistently shows smaller biases compared to the CNTL experiment (not shown),  
27 which implies that the model representation of CO<sub>2</sub> at JR-STATION sites is more accurate in  
28 the JR experiment than in the CNTL experiment. Model CO<sub>2</sub> concentrations calculated by  
29 background surface CO<sub>2</sub> fluxes in the JR experiment are also more consistent with the  
30 observations, implying that background scaling factors of the JR experiment are more  
31 accurate than those of the CNTL experiment. The background surface CO<sub>2</sub> fluxes are  
32 calculated by multiplying the background scaling factor to prior biosphere and ocean fluxes as

1 in Eq. (1). In addition, the average innovation  $\chi^2$ -statistics at the JR-STATION sites are  
2 generally close to 1, implying that the defined MDM is an appropriate value. Therefore, by  
3 assimilating JR-STATION observation data, the JR experiments exhibits better results than  
4 the CNTL experiment at observation sites in EB.

5 However, at observation sites in ET and Europe, the difference in biases of the two  
6 experiments is relatively small and not significant enough to determine which experiment  
7 exhibits better results. This is due to the small difference of optimized surface CO<sub>2</sub> fluxes  
8 between the two experiments in the ET region. The observation sites in Europe are located far  
9 from Eastern Europe and Siberia as shown in Fig. 1 so that they are not sensitive to the  
10 change of surface CO<sub>2</sub> uptake in those regions. In addition, the MDM at four sites (BAL, BSC,  
11 HUN, and OBN) in Europe is assigned as 7.5 ppm, the largest value in CarbonTracker, due to  
12 poor representation of the transport model at these sites (Peters et al., 2010).

13 "In addition, model CO<sub>2</sub> concentrations calculated by optimized fluxes of the two  
14 experiments are compared with independent, not assimilated, vertical profiles of CO<sub>2</sub>  
15 concentration measurements by aircraft at BRZ site in Siberia. Aircraft measurements were  
16 conducted in the afternoon on good weather days. The frequency of flight was usually two to  
17 four times per month (Sasakawa et al., 2013). Table 5 presents the average bias, root-mean-  
18 square difference (RMSD), mean absolute error (MAE), and Pearson's correlation coefficient  
19 of the model CO<sub>2</sub> concentrations calculated by optimized fluxes of the two experiments based  
20 on the observations at BRZ site as the reference. The statistics are calculated at each vertical  
21 bin with 500 meter interval by using aircraft measurements observed between 1200 – 1600  
22 LST. Overall, the biases of two experiments are less than 0.80 ppm showing good consistency  
23 between model and observed CO<sub>2</sub> concentrations. Near the surface, the result of JR  
24 experiment is better than that of CNTL experiment in terms of bias. The bias of the JR  
25 experiment is smaller than those of the CNTL experiment at the level under 500 m, whereas  
26 the biases of the CNTL experiment are smaller than those of the JR experiment at the levels  
27 above 500 m. The more CO<sub>2</sub> concentrations are generated over BRZ site because of the  
28 reduced uptake of surface CO<sub>2</sub> fluxes over Siberia in JR experiment. The standard deviations  
29 of the CNTL experiment are greater than those of JR experiment, which implies that the  
30 biases of the CNTL experiment fluctuate as its average more than those of the JR experiment.  
31 In contrast, the RMSD and MAE of the JR experiment are smaller than those of the CNTL  
32 experiment, and the correlation coefficient of the JR experiment is greater than that of the

1 CNTL experiments. Therefore, overall the statistics show that the model CO<sub>2</sub> concentrations  
2 of the JR experiment is relatively more consistent with independent CO<sub>2</sub> concentration  
3 observations compared to those of the CNTL experiment over Siberia.”

### 4 **3.3 Uncertainty reduction and observation impact**

5 The effects of additional observations on the optimized surface CO<sub>2</sub> flux and associated  
6 uncertainties are investigated. Figure 7 shows the average, average in summer (June, July, and  
7 August) and average in winter (December, January, February) uncertainty reductions from  
8 2002 to 2009. The uncertainty reduction based on the uncertainty of CNTL as the reference is  
9 calculated as

$$10 \quad UR = \frac{\sigma_{CNTL} - \sigma_{JR}}{\sigma_{CNTL}} \times 100(\%), \quad (8)$$

11 where  $\sigma_{CNTL}$  and  $\sigma_{JR}$  are one-sigma standard deviations of the optimized scaling factor for  
12 CNTL experiment and JR experiment, respectively, assuming Gaussian errors. The maximum  
13 uncertainty reduction is the greatest value in any week in the period 2002 to 2009 in each  
14 ecoregion. As expected, the average uncertainty reduction is readily apparent in the Conifer  
15 Forest of EB in which JR stations are mainly located, which has the additional observations  
16 (Fig. 7a). The uncertainty reduction of Asia and Europe, especially in the forest of Siberia and  
17 Eastern Europe, is greater than for other regions. The spatial pattern of the maximum  
18 uncertainty reduction is similar to that of the average values (not shown). The uncertainty  
19 reduction of EB in summer is higher than that in winter (Figs. 7b, c) due to a higher  
20 uncertainty associated with larger net fluxes in summer compared to winter (Fig. 6a). For  
21 example, the average value of the Conifer Forest of EB is 29.1%, the maximum value is  
22 78.6%, the average value in summer is 36.3% and the average value in winter is 29.7%,  
23 respectively. The uncertainty reduction of CNTL and JR experiments based on the prior  
24 uncertainty as the reference ( $\sigma_{prior}$  used instead of  $\sigma_{CNTL}$  in Eq. (8);  $\sigma_{CNTL}$  or  $\sigma_{JR}$  used instead  
25 of  $\sigma_{JR}$  in Eq. (8)) shows similar values in the NH except in Siberia region (not shown). In  
26 addition, the difference between average uncertainty reduction of CNTL and JR experiments  
27 based on the prior uncertainty as the reference (not shown) is very similar to the average of  
28 uncertainty reduction in Eq. (8) shown in Fig.7a. Therefore, the uncertainties of the optimized  
29 surface CO<sub>2</sub> fluxes are reduced by the additional observations.

1 To investigate the impact of individual observations on the optimized surface CO<sub>2</sub> flux, the  
2 self-sensitivities are calculated by the method demonstrated by Kim et al. (2014b). The self-  
3 sensitivity is the diagonal element of the influence matrix which measures the impact of  
4 individual observations in the observation space on the optimized surface CO<sub>2</sub> flux. The large  
5 self-sensitivity value implies that the information extracted from observations is large. Figure  
6 8 shows the self-sensitivities of the two experiments averaged from 2002 to 2009. The  
7 average self-sensitivities at the JR-STATION sites are approximately 60% larger than those at  
8 the towers in North America, i.e., continuous site category observations in Fig. 1. The global  
9 average self-sensitivities are 4.83% (CNTL experiment) and 5.08% (JR experiment), and the  
10 cumulative impacts for the 5 weeks assimilation window are 18.79% (CNTL experiment) and  
11 19.33% (JR experiment). The average self-sensitivities of additional observations are higher  
12 than those of other sites, providing much information for estimating surface CO<sub>2</sub> fluxes. In  
13 particular, YAK site located in east Siberia provides greater impacts than other JR-STATION  
14 sites located in 60 ~ 90°E.

15 The RMSDs between the optimized surface CO<sub>2</sub> fluxes and the background fluxes at each  
16 assimilation step in summer are calculated (Fig. 9). The RMSD of the analyzed surface CO<sub>2</sub>  
17 fluxes constrained by one week of observations from the background fluxes in JR experiment  
18 is greater than that in CNTL experiment (Figs. 9a, b), implying that surface CO<sub>2</sub> fluxes in  
19 Siberia are analyzed by JR-STATION data in Siberia directly at the first cycle. This is  
20 consistent with the high value of self-sensitivities at JR-STATION sites as shown in Fig. 8b.  
21 Because JR-STATION data are abundant and have large self-sensitivities, these observations  
22 provide large information on the estimated surface CO<sub>2</sub> fluxes over Siberia in the first cycle.  
23 Kim et al. (2014b) showed that the RMSD in Asia increases after 5 weeks of optimization,  
24 which implies that it takes more than 1 week to affect the surface CO<sub>2</sub> fluxes in Siberia by the  
25 transport of the CO<sub>2</sub> concentrations observed in remote regions. However, by assimilating the  
26 CO<sub>2</sub> concentrations observed at the JR-STATION sites in Siberia, the observation impact on  
27 the optimized surface CO<sub>2</sub> fluxes in Siberia increases after 1 week of optimization (Fig. 9b).  
28 In contrast, the RMSD in the Siberia region increases after 5 weeks of optimization in the  
29 CNTL experiment compared to that in the JR experiment (Figs. 9c, d), which corresponds to  
30 the reduced uptake of optimized surface CO<sub>2</sub> fluxes in JR experiment as shown in Fig. 2b.



### 1 3.4 Comparison with other results

2 A comparison of the optimized surface CO<sub>2</sub> flux in this study with other previous studies is  
3 presented in Table 6. In the EB, the land sink from the JR experiment ( $-0.77 \pm 0.70$  Pg C yr<sup>-1</sup>)  
4 is smaller than those reported by Zhang et al. (2014b) ( $-1.02 \pm 0.91$  Pg C yr<sup>-1</sup>), Maki et al.  
5 (2010) ( $-1.46 \pm 0.41$  Pg C yr<sup>-1</sup>), and the CT2013B (CarbonTracker released on 9 February  
6 2015; documented online at <http://www.esrl.noaa.gov/gmd/ccgg/carbontracker/CT2013B/>)  
7 results ( $-1.00 \pm 3.75$  Pg C yr<sup>-1</sup>), but higher than those reported by Saeki et al. (2013) ( $-$   
8  $0.35 \pm 0.61$  Pg C yr<sup>-1</sup>; including biomass burning  $0.11$  Pg C yr<sup>-1</sup>), and similar with those  
9 reported by Dolman et al. (2012) ( $-0.613$  Pg C yr<sup>-1</sup>).

10 Because CT2013B and Zhang et al. (2014b) use the similar inversion framework as this study,  
11 the reduced land sink is caused by assimilating additional observations. The difference in land  
12 sink between the JR experiment and Saeki et al. (2013) is caused by a different inversion  
13 system framework which includes prior flux information, atmospheric transport model,  
14 observation data set, and inversion method. Despite different inversion system framework  
15 used in each study, two studies using the JR-STATION data exhibit similar results in relative  
16 terms, reduced uptake of CO<sub>2</sub> fluxes and uncertainties over Siberia. Nonetheless, the land sink  
17 from the JR experiment is somewhat different with other inversion results, its value falls  
18 within the flux uncertainty range. Although the land sink in Dolman et al. (2012) is the  
19 average land sink obtained from three methods (inventory-based, eddy covariance, and  
20 inversion methods) and estimated not only for Siberia but for Russian territory including  
21 Ukraine, Belarus, and Kazakhstan, the land sinks of the JR experiment and Dolman et al.  
22 (2012) shows similar values. Overall, the optimized surface CO<sub>2</sub> fluxes in EB of JR  
23 experiment are comparable to those of other previous studies.

24 In Europe, though the long-term average land sink from the JR experiment ( $-0.37 \pm 0.64$  Pg C  
25 yr<sup>-1</sup>) is higher than that of CTE2014 ( $-0.07 \pm 0.49$  Pg C yr<sup>-1</sup>), the average land sink from 2008-  
26 2009 of the JR experiment ( $-0.75 \pm 0.63$  Pg C yr<sup>-1</sup>) is much higher than that of CTE2014 ( $-$   
27  $0.11 \pm 0.38$  Pg C yr<sup>-1</sup>). The land sinks of the JR experiment in 2008 and 2009 are  $-0.73 \pm 0.41$   
28 and  $-0.76 \pm 0.38$  Pg C yr<sup>-1</sup>, respectively, whereas much lower uptakes ( $-0.21 \pm 0.49$ ,  $-0.38 \pm 0.44$   
29 Pg C yr<sup>-1</sup>) are obtained for the CNTL experiment. According to Reuter et al. (2014), despite  
30 the different experiment period, the land sink of Europe in 2010 ( $-1.02 \pm 0.30$  Pg C yr<sup>-1</sup>)  
31 estimated by using satellite observations is much higher than previous inversion studies (e.g.,  
32 Peylin et al. 2013) using only surface observations.

1

## 2 **4 Summary and conclusions**

3 In this study, to investigate the effect of the Siberian observations, which are not used in the  
4 previous studies using CarbonTracker, on the optimization of surface CO<sub>2</sub> fluxes, two  
5 experiments, named CNTL and JR, with different sets of observations from 2000 to 2009  
6 were conducted and optimized surface CO<sub>2</sub> fluxes from 2002 to 2009 were analyzed.

7 The global balances of the sources and sinks of surface CO<sub>2</sub> fluxes were maintained with a  
8 similar trend for both experiments, while the distribution of the optimized surface CO<sub>2</sub> fluxes  
9 changed. The magnitude of the optimized biosphere surface CO<sub>2</sub> uptake and its uncertainty in  
10 EB (Siberia) was decreased from  $-1.17 \pm 0.93$  Pg C yr<sup>-1</sup> to  $-0.77 \pm 0.70$  Pg C yr<sup>-1</sup>, whereas it was  
11 increased in other regions of the NH (Eurasian Temperate, Europe, North American Boreal,  
12 and North American Temperate). The land sink of Europe increased significantly for 2008  
13 and 2009, which is consistent with the other inversion results inferred by satellite observations.  
14 Additional observations are used to correct the surface CO<sub>2</sub> uptake in June and July, the active  
15 vegetation uptake season, in terms of monthly average optimized surface CO<sub>2</sub> fluxes. As a  
16 result, the additional observations do not exhibit a change in the magnitude of the global  
17 surface CO<sub>2</sub> flux balance because they provide detailed information about the Siberian land  
18 sink instead of the global land sink magnitude, when they are used in the well-constructed  
19 inversion modeling system.

20 The model CO<sub>2</sub> concentration using the background and optimized surface CO<sub>2</sub> fluxes in the  
21 JR experiment are more consistent with the CO<sub>2</sub> observations used in the optimization than  
22 those in the CNTL experiment, showing lower biases in the EB region. In contrast, the  
23 differences of biases in ET and Europe between the two experiments are not distinguishable.  
24 In comparison with vertical profiles of CO<sub>2</sub> concentration observations which are not used in  
25 the optimization, the model CO<sub>2</sub> concentrations in the JR experiment show the smaller RMSD  
26 and MAE, and the greater correlation coefficient than those in CNTL experiment.

27 The new observations provide useful information on the optimized surface CO<sub>2</sub> fluxes. The  
28 observation impact of the Siberian observation data is investigated by means of uncertainty  
29 reduction and self-sensitivity calculated by an influence matrix. Additional observations  
30 reduce the uncertainty of the optimized surface CO<sub>2</sub> fluxes in Asia and Europe, mainly in the  
31 EB (Siberia), where the new observations are used in the assimilation. The average self-  
32 sensitivities of the JR-STATION sites are approximately 60% larger than those at other

1 continuous measurements (e.g., tower measurements in North America). The global average  
2 self-sensitivity and cumulative impact of the JR experiment are higher than that of the CNTL  
3 experiment, which implies that the individual observation impact of JR-STATION data on  
4 optimized surface CO<sub>2</sub> fluxes is higher than the average values. The RMSD of the analyzed  
5 surface CO<sub>2</sub> fluxes constrained by one week of observations from the background fluxes also  
6 suggests that new Siberian observations provide a larger amount of information on the  
7 optimized surface CO<sub>2</sub> fluxes.

8 This study shows that the JR-STATION data affect the longitudinal distribution of the total  
9 NH sinks, especially in the EB and Europe, when it is used by atmospheric CO<sub>2</sub> inversion  
10 modeling. In the future, it is expected that Siberian observations will be used as an important  
11 constraint for estimating surface CO<sub>2</sub> fluxes over the NH with various CO<sub>2</sub> observations (e.g.  
12 satellite and aircraft measurements) simultaneously.

### 13 **Acknowledgements**

14 The authors appreciate Dr. Abhishek Chatterjee and other reviewers for their valuable  
15 comments. This study was funded by the Korea Meteorological Administration Research and  
16 Development Program under the Grant KMIPA 2015-2021. The JR-STATION is supported  
17 by the Global Environment Research Account for National Institutes of the Ministry of the  
18 Environment, Japan and the Russian Foundation for Basic Research (Grant No. 14-05-00590).  
19 The authors also acknowledge atmospheric CO<sub>2</sub> measurements data providers and  
20 cooperating agencies at China Meteorological Administration, Commonwealth Scientific and  
21 Industrial Research Organization, Environment Canada, Finnish Meteorological Institute,  
22 Hungarian Meteorological Service, Japan Meteorological Agency, Lawrence Berkeley  
23 National Laboratory, National Institute of Environmental Research, Norwegian  
24 Meteorological Institute, Max Planck Institute for Biogeochemistry, Morski Instytut Rybacki,  
25 National Center for Atmospheric Research, National Oceanic and Atmospheric  
26 Administration Earth System Research Laboratory, and Romanian Marine Research Institute.  
27

## 1 **References**

- 2 Berchet, A., Pison, I., Chevallier, F., Bousquet, P., Bonne, J.-L., and Paris, J.-D.: Objectified  
3 quantification of uncertainties in Bayesian atmospheric inversions, *Geosci. Model. Dev.*, 8,  
4 1525-1546, doi:10.5194/gmd-8-1525-2015, 2015a.
- 5 Berchet, A., Pison, I., Chevallier, F., Paris, J.-D., Bousquet, P., Bonne, J.-L., Arshinov, M. Y.,  
6 Belan, B. D., Cressot, C., Davydov, D. K., Dlugokencky, E. J., Fofonov, A. V., Galanin, A.,  
7 Lavrič, J., Machida, T., Parker, R., Sasakawa, M., Spahni, R., Stocker, B. D., and Winderlich,  
8 J.: Natural and anthropogenic methane fluxes in Eurasia: a mesoscale quantification by  
9 generalized atmospheric inversion, *Biogeosciences*, 12, 5393-5414, doi:10.5194/bg-12-5393-  
10 2015, 2015b.
- 11 Boden, T., Marland, G., and Andres, R.: Global, regional, and national fossil-fuel CO<sub>2</sub>  
12 emissions, Carbon Dioxide Information Analysis Center, Oak Ridge National Laboratory, US  
13 Department of Energy, Oak Ridge, Tenn., USA doi:10.3334/CDIAC/00001\_V2010, 10, 2010.
- 14 Bruhwiler, L. M. P., Michalak, A. M., and Tans, P. P.: Spatial and temporal resolution of  
15 carbon flux estimates for 1983-2002, *Biogeosciences*, 8, 1309-1331, doi:10.5194/bg-8-1309-  
16 2011, 2011.
- 17 Ciais, P., Reichstein, M., Viovy, N., Granier, A., Ogée, J., Allard, V., Aubinet, M., Buchmann,  
18 N., Bernhofer, Chr., Carrara, A., Chevallier, F., De Noblet, N., Friend, A. D., Friedlingstein,  
19 P., Grünwald, T., Heinesch, B., Keronen, P., Knohl, A., Krinner, G., Loustau, D., Manca, G.,  
20 Matteucci, G., Miglietta, F., Ourcival, J. M., Papale, D., Pilegaard, K., Rambal, S., Seufert, G.,  
21 Soussana, J. F., Sanz, M. J., Schulze, E. D., Vesala, T., and Valentini, R.: Europe-wide  
22 reduction in primary productivity caused by the heat and drought in 2003, *Nature*, 529-533,  
23 doi:10.1038/natures03972, 2005.
- 24 Chevallier, F., Bréon, F.-M., and Rayner, P. J.: Contribution of the Orbiting Carbon  
25 Observatory to the estimation of CO<sub>2</sub> sources and sinks: Theoretical study in a variational  
26 data assimilation framework, *J. Geophys. Res. Atmos.*, 112, D09307,  
27 doi:10.1029/2006JD007375, 2007.
- 28 Chevallier, F., Ciais, P., Conway, T. J., Aalto, T., Anderson, B. E., Bousquet, P., Brunke, E.  
29 G., Ciattaglia, L., Esaki, Y., Fröhlich, M., Gomez, A., Gomez-Pelaez, A. J., Haszpra, L.,  
30 Krummel, P. B., Langenfelds, R. L., Leuenberger, M., Machida, T., Maignan, F., Matsueda,  
31 H., Morguí, J. A., Mukai, H., Nakazawa, T., Peylin, P., Ramonet, M., Rivier, L., Sawa, Y.,

1 Schmdit, M., Steele, L. P., Vay, S. A., Vermeulen, A. T., Wofsy, S., and Worthy, D.: CO<sub>2</sub>  
2 surface fluxes at grid point scale estimated from a global 21 year reanalysis of atmospheric  
3 measurements, *J. Geophys. Res. Atmos.*, 115, D21307, doi 10.1029/2010jd013887, 2010.

4 Dolman, A. J., Shvidenko, A., Schepaschenko, D., Ciais, P., Tchepakova, N., Chen, T., van  
5 der Molen, M. K., Belelli Marchesini, L., Maximov, T. C., Maksyutov, S., and Schulze, E.-  
6 D.: An estimate of the terrestrial carbon budget of Russia using inventory-based, eddy  
7 covariance and inversion methods, *Biogeosciences*, 9, 5323-5340, doi:10.5194/bg-9-5323-  
8 2012, 2012.

9 Engelen, R. J., Denning, A. S., Gurney, K. R., and TransCom3 modelers: On error estimation  
10 in atmospheric CO<sub>2</sub> inversions, *J. Geophys. Res.*, 107, 4635, doi:10.1029/2002JD002195,  
11 2002.

12 European Commission: Joint Research Centre (JRC)/Netherlands Environmental Assessment  
13 Agency (PBL): Emission Database for Global Atmospheric Research (EDGAR), release  
14 version 4.0, 2009.

15 Feng, L., Palmer, P. I., Parker, R. J., Deutscher, N. M., Feist, D. G., Kivi, R., Morino, I. and  
16 Sussmann, R.: Estimates of European uptake of CO<sub>2</sub> inferred from GOSAT XCO<sub>2</sub> retrievals:  
17 sensitivity to measurement bias inside and outside Europe, *Atmos. Chem. Phys.*, 16, 1289-  
18 1302, doi:10.5194/acp-16-1289-2016, 2016.

19 Gurney, K. R., Law, R. M., Denning, A. S., Rayner, P. J., Baker, D., Bousquet, P., Bruhwiler,  
20 L., Chen, Y. H., Ciais, P., Fan, S., Fung, I. Y., Gloor, M., Heimann, M., Higuchi, K., John, J.,  
21 Maki, T., Maksyutov, S., Masarie, K., Peylin, P., Prather, M., Pak, B. C., Randerson, J.,  
22 Sarmiento, J., Taguchi, S., Takahashi, T., and Yuen, C. W.: Towards robust regional  
23 estimates of CO<sub>2</sub> sources and sinks using atmospheric transport models, *Nature*, 415, 626–630,  
24 2002.

25 Hayes, D. J., McGuire, A. D., Kicklighter, D. W., Gurney, K. R., Burnside, T. J., and Melillo,  
26 J. M.: Is the northern high-latitude land-based CO<sub>2</sub> sink weakening?, *Global Biogeochem. Cy.*,  
27 25, GB3018, doi:10.1029/2010GB003813, 2011.

28 Houghton, R. A., Butman, D., Bunn, A. G., Krankina, O. N., Schlesinger, P., and Stone, T.  
29 A.: Mapping Russian forest biomass with data from satellites and forest inventories. *Environ.*  
30 *Res. Lett.*, 2, 045032, doi:10.1088/1748-9326/2/4/045032, 2007.

1 Houtekamer, P. L., and Mitchell, H. L.: A sequential ensemble Kalman filter for atmospheric  
2 data assimilation, *Mon. Wea. Rev.*, 129, 123-137, 2001.

3 Jacobson, A. R., Mikaloff Fletcher, S. E., Gruber, N., Sarmiento, J. L., and Gloor, M.: A joint  
4 atmosphere–ocean inversion for surface fluxes of carbon dioxide: 1. Methods and global-scale  
5 fluxes, *Global Biogeochem. Cy.*, 21, B1019, doi:10.1029/2005GB002556, 2007.

6 Kim, J., Kim, H. M., and Cho, C.-H.: Application of Carbon Tracking System based on  
7 ensemble Kalman Filter on the diagnosis of Carbon Cycle in Asia, *Atmosphere*, 22(4), 415-  
8 447, 2012. (in Korean with English abstract)

9 Kim, J., Kim, H. M., and Cho, C.-H.: The effect of optimization and the nesting domain on  
10 carbon flux analyses in Asia using a carbon tracking system based on the ensemble Kalman  
11 filter, *Asia-Pacific J. Atmos. Sci.*, 50, 327-344, doi:10.1007/s13143-014-0020-7, 2014a.

12 Kim, J., Kim, H. M., and Cho, C.-H.: Influence of CO<sub>2</sub> observations on the optimized CO<sub>2</sub>  
13 flux in an ensemble Kalman filter, *Atmos. Chem. Phys.*, 14, 13515-13530, doi:10.5194/acp-  
14 14-13515-2014, 2014b.

15 Knorr, W., Gobron, N., Scholze, M., Kaminski, T., Schnur, R., and Pinty, B.: Impact of  
16 terrestrial biosphere carbon exchanges on the anomalous CO<sub>2</sub> increase in 2002-2003,  
17 *Geophys. Res. Lett.*, 34, L09703, doi:10.1029/2006GL029019, 2007.

18 Krol, M., Houweling, S., Bregman, B., Broek, M., van der Segers, A., Velthoven, P. V.,  
19 Peters, W., Dentener, F., and Bergamaschi, P.: The two-way nested global chemistry-  
20 transport zoom model TM5: Algorithm and applications, *Atmos. Chem. Phys.*, 5, 417-432,  
21 2005.

22 Kurganova, I. N., Kudryarov, V. N., and Lopes De Gerenyu, V. O.: Updated estimate of  
23 carbon balance on Russian territory, *Tellus*, 62B, 497-505, doi:10.1111/j.1600-  
24 0889.2010.00467.x, 2010.

25 Le Quéré, C., Moriarty, R., Andrew, R. M., Peters, G. P., Ciais, P., Friedlingstein, P., Jones, S.  
26 D., Sitch, S., Tans, P., Arneeth, A., Boden, T. A., Bopp, L., Bozec, Y., Canadell, J. G., Chini, L.,  
27 P., Chevallier, F., Cosca, C. E., Harris, I., Hoppema, M., Houghton, R. A., House, J. I., Jain,  
28 A. K., Johannessen, T., Kato, E., Keeling, R. F., Kitidis, V., Klein Goldewijk, K., Koven, C.,  
29 Landa, C. S., Landschützer, P., Lenton, A., Lima, I. D., Marland, G., Mathis, J. T., Metzl, N.,  
30 Nojiri, Y., Olsen, A., Ono, T., Peng, S., Peters, W., Pfeil, B., Poulter, B., Raupach, M. R.,  
31 Regnier, P., Rödenbeck, C., Saito, S., Salisbury, J. E., Schuster, U., Schwinger, J., Séférian,

1 R., Segschneider, J., Steinhoff, T., Stocker, B. D., Sutton, A. J., Takahashi, T., Tilbrook, B.,  
2 van der Werf, G. R., Viovy, N., Wang, Y.-P., Wanninkhof, R., Wiltshire, A., and Zeng, N.:  
3 Global carbon budget 2014, *Earth Syst. Sci. Data*, 7, 47–85, doi:10.5194/essd-7-47-2015,  
4 2015.

5 Lloyd, J., Langenfelds, R. L., Francey, R. J., Gloor, M., Tchebakova, N. M., Zolotoukhine, D.,  
6 Brand, W. A., Werner, R. A., Jordan, A., Allison, C. A., Zrazhewske, V., Shibistova, O., and  
7 Schulze, E.-D.: A trace-gas climatology above Zotino, central Siberia, *Tellus*, 54B, 749-767,  
8 2002.

9 Machida, T., Matsueda, H., Sawa, Y., Nakagawa, Y., Hirofani, K., Kondo, N., Goto, K.,  
10 Nakazawa, T., Ishikawa, K., and Ogawa, T.: Worldwide Measurements of Atmospheric CO<sub>2</sub>  
11 and Other Trace Gas Species Using Commercial Airlines, *J. Atmos. Oceanic Techno.*, 25,  
12 1744-1754, doi:10.1175/2008JTECHA1082.1, 2008.

13 Machida, T., Tohjima, Y., Katsumata, K., and Mukai, H.: A new CO<sub>2</sub> calibration scale based  
14 on gravimetric one-step dilution cylinders in National Institute for Environmental Studies-  
15 NIES 09 CO<sub>2</sub> scale, Report of the 15th WMO/IAEA Meeting of Experts on Carbon Dioxide,  
16 Other Related Tracer Measurement Techniques, GAW Rep. 194, 165-169, World  
17 Meteorological Organization, Geneva, Switzerland, 2011.

18 Maki, T., Ikegami, M., Fujita, T., Hirahara, T., Yamada, K., Mori, K., Takeuchi, A., Tsutsumi,  
19 Y., Suda, K., and Conway, T. J.: New technique to analyse global distributions of CO<sub>2</sub>  
20 concentrations and fluxes from non-processed observational data, *Tellus*, 62B, 797-809,  
21 doi:10.1111/j.1600-0889.2010.00488.x, 2010.

22 Maksyutov, S., Machida, T., Mukai, H., Patra, P. K., Nakazawa, T., Inoue, G., and Transcom-  
23 3 Modelers: Effect of recent observations on Asia CO<sub>2</sub> flux estimates by transport model  
24 inversions, *Tellus*, 55B, 522-529, 2003.

25 Masarie, K. A., Peters, W., Jacobson, A. R., and Tans, P. P.: ObsPack: a framework for the  
26 preparation, delivery, and attribution of atmospheric greenhouse gas measurements, *Earth*  
27 *Syst. Sci. Data*, 6, 375-384, doi:10.5194/essd-6-375-2014, 2014.

28 Miller, C. E., Crisp, D., DeCola, P. L., Olsen, S. C., Randerson, J. T., Michalak, A. M.,  
29 Alkhaled, A., Rayner, P., Jacob, D. J., Suntharalingam, P., Jones, D. B. A., Denning, A. S.,  
30 Nicholls, M. E., Doney, S. C., Pawson, S., Boesch, H., Connor, B. J., Fung, I. Y., O'Brien, D.  
31 O., Salawitch, R. J., Sander, S. P., Sen, B., Tans, P., Toon, G. C., Wennberg, P. O., Wofsy, S.

1 C., Yung, Y. L., and Law, R. M.: Precision requirements for space-based XCO<sub>2</sub> data, *J.*  
2 *Geophys. Res.*, 112, D10314, doi:10.1029/2006JD007659, 2007.

3 Olson, J., Watts, J., and Allsion, L.: Major World Ecosystem Complexes Ranked by Carbon  
4 in Live Vegetation: a Database, Tech. rep., Carbon Dioxide Information Analysis Center, U.S.  
5 Department of Energy, Oak Ridge National Laboratory, Oak Ridge, Tennessee, USA,  
6 doi:10.3334/CDIAC/lue.ndp017, 1992.

7 Olsen, S. C., and Randerson, J. T.: Differences between surface and column atmospheric CO<sub>2</sub>  
8 and implications for carbon cycle research, *J. Geophys. Res.*, 109, D02301,  
9 doi:10.1029/2003JD003968, 2004.

10 Paris, J.-D., Ciais, P., Nédélec, P., Ramonet, M., Belan, B. D., Arshinov, M. Y., Golitsyn, G.  
11 S., Granberg, I., Stohl, A., Cayez, G., Athier, G., Boumard, F., and Cousin, J. M.: The YAK-  
12 AEROSIB transcontinental aircraft campaigns: new insights on the transport of CO<sub>2</sub>, CO and  
13 O<sub>3</sub> across Siberia, *Tellus B*, 60, 551– 568, 2008.

14 Peters, W., Jacobson, A. R., Sweeney, C., Andrews, A. E., Conway, T. J., Masarie, K., Miller,  
15 J. B., Bruhwiler, L. M. P., Petron, G., Hirsch, A. I., Worthy, D. E. J., van der Werf, G. R.,  
16 Randerson, J. T., Wennberg, P. O., Krol, M. C., Tans, P. P.: An atmospheric perspective on  
17 North American carbon dioxide exchange: CarbonTracker, *Proc. Nat. Acad. Sci. U.S.A.*, 104,  
18 18925-18930, 2007.

19 Peters, W., Krol, M. C., van der Werf, G. R., Houweling, S., Jones, C. D., Hughes, J.,  
20 Schaefer, K., Masarie, K. A., Jacobson, A. R. Miller, J. B., Cho, C. H., Ramonet, M., Schmidt,  
21 M., Ciattaglia, L., Apadula, F., Heltai, D., Meinhardt, F., di Sarra, A. G., Piacentino, S.,  
22 Sferlazzo, D., Aalto, T., Hatakka, J., Ström, J., Haszpra, L., Meijer, H. A. J., van der Laan, S.,  
23 Neubert, R. E. M., Jordan, A., Rodó, X., Morguí, J. A., Vermeulen, A. T., Popa, E., Rozanski,  
24 K., Zimnoch, M., Manning, A. C., Leuenberger, M., Uglietti, C., Dolman, A. J., Ciais, P.  
25 Heimann, M., and Tans, P. P.: Seven years of recent European net terrestrial carbon dioxide  
26 exchange constrained by atmospheric observations, *Global Change Biol.*, 16, 1317-1337,  
27 doi:10.1111/j.1365-2486.2009.02078.x, 2010.

28 Peylin P., Law, R. M., Gurney, K. R., Chevallier, F., Jacobson A. R., Maki, T., Niwa, Y.,  
29 Patra, P. K., Peters, W., Rayner, P. J., Rödenbeck, C., van der Laan-Luijkx, I. T., and Zhang,  
30 X.: Global atmospheric carbon budget: results from an ensemble of atmospheric CO<sub>2</sub>  
31 inversions, *Biogeosciences*, 10, 6699-6720, doi:10.5194/bg-10-6699-2013, 2013.



1 Quegan, S., Beer, C., Shvidenko, A., McCallum, I., Handoh, I. C., Peylin, P., Rödenbeck, C.,  
2 Lucht, W., Nilsson, S., and Schmullius, C.: Estimating the carbon balance of central Siberia  
3 using landscape-ecosystem approach, atmospheric inversion and dynamic global vegetation  
4 models, *Glob. Change Biol.*, 17, 351-365, doi:10.1111/j.1365-2486.2010.02275.x, 2011.

5 Reuter, M., Buchwitz, M., Hilker, M., Heymann, J., Schneising, O., Pillai, D., Bovensmann,  
6 H., Burrows, J. P., Bösch, H., Parker, R., Butz, A., Hasekamp, O., O'Dell, C. W., Yoshida, Y.,  
7 Gerbig, C., Nehr Korn, T., Deutscher, N. M., Warneke, T., Notholt, J., Hase, F., Kivi, R.,  
8 Sussmann, R., Machida, T., Matsueda, H., and Sawa, Y.: Satellite-inferred European carbon  
9 sink larger than expected, *Atmos. Chem. Phys.*, 14, 13739-13753, doi:10.5194/acp-14-13739-  
10 2014, 2014.

11 Saeki, T., Maksyutov, S., Sasakawa, M., Machida, T., Arshinov, M., Tans, P. P., Conway, T.  
12 J., Saito, M., Valsala, V., Oda, T., Andres, R. J., and Belikov, D.: Carbon flux estimation for  
13 Siberia by inverse modeling constrained by aircraft and tower CO<sub>2</sub> measurements, *J. Geophys.*  
14 *Res. Atmos.*, 118, 1100-1122, doi:10.1002/jgrd.50127, 2013.

15 Sasakawa, M., Shimoyama, K., Machida, T., Tsuda, N., Suto, H., Arshinov, M., Davydov, D.,  
16 Fofonov, A., Krasnov, O., Saeki, T., Koyama, Y., and Maksyutov, S.: Continuous  
17 measurements of methane from a tower network over Siberia, *Tellus*, 62B, 403-416,  
18 doi:10.1111/j.1600-0889.2010.00494.x, 2010.

19 Sasakawa, M., Machida, T., Tsuda, N., Arshinov, M., Davydov, D., Fofonov, A., and  
20 Krasnov, O.: Aircraft and tower measurements of CO<sub>2</sub> concentration in the planetary  
21 boundary layer and the lower free troposphere over southern taiga in West Siberia: Long-term  
22 records from 2002 to 2011, *J. Geophys. Res. Atmos.*, 118, 9489-9498,  
23 doi:10.1002/jgrd.50755, 2013.

24 Schepaschenko, D., McCallum, I., Shvidenko, A., Fritz, S., Kraxner, F., and Obersteiner, M. :  
25 A new hybrid land cover dataset for Russia: a methodology for integrating statistics, remote  
26 sensing and in situ information, *J. Land Use Sci.*, 6, 245-259,  
27 doi:10.1080/1747423X.2010.511681, 2011.

28 Schneising, O., Buchwitz, M., Reuter, M., Heymann, J., Bovensmann, H., and Burrows, J. P.:  
29 Long-term analysis of carbon dioxide and methane column-averaged mole fractions retrieved  
30 from SCIAMACHY, *Atmos. Chem. Phys.*, 11, 2863-2880, doi:10.5194/acp-11-2863-2011,  
31 2011

1 Schulze, E.-D., Lloyd, J., Kelliher, F. M., Wirth, C., Rebmann, C., Lühker, B., Mund, M.,  
2 Knohl, A., Milyukova, I. M., Schulze, W., Ziegler, W., Varlagin, A. B., Sogachev, A. F.,  
3 Valentini, R., Dore, S., Grigoriev, S., Kolle, O., Panfyorov, M. I., Tchebakova, N., and  
4 Vygodskaya, N. N.: Productivity of forests in the Eurosiberian boreal region and their  
5 potential to act as a carbon sink – a synthesis. *Glob. Change Biol.*, 5, 703-722,  
6 doi:10.1046/j.1365-2486.1999.00266.x, 1999.

7 Tarnocai, C., Canadell, J. G., Schuur, E. A. G., Kuhry, P., Mazhitova, G., and Zimov, S.: Soil  
8 organic carbon pools in the northern circumpolar permafrost region, *Glob. Biogeochem.*  
9 *Cycles*, 23, GB2023, doi:10.1029/2008GB003327, 2009.

10 Turnbull, J. C., Miller, J. B., Lehman, S. J., Hurst, D., Peters, W., Tans, P. P., Southon, J.,  
11 Montzka, S. A., Elkins, J. W., Mondeel, D. J., Romashkin, P. A., Elansky, N., and  
12 Skorokhod, A.: Spatial distribution of  $\Delta^{14}\text{CO}_2$  across Eurasia: measurements from the  
13 TROICA-8 expedition, *Atmos. Chem. Phys.*, 9, 175-187, doi:10.5194/acp-9-175-2009, 2009.

14 van der Laan-Luijkx, I. T., van der Velde, I. R., Krol, M. C., Gatti, L. V., Domingues, L. G.,  
15 Correia, C. S. C., Miller, J. B., Gloor, M., van Leeuwen, T. T., Kaiser, J. W., Wiedinmyer, C.,  
16 Basu, S., Clerbaux, C., and Peters, W.: Response of the Amazon carbon balance to the 2010  
17 drought derived with CarbonTracker South America, *Global Biogeochem. Cycles*, 29, 1092-  
18 1108, doi:10.1002/2014GB005082, 2015.

19 van der Werf, G. R., Randerson, J. T., Giglio, L., Collatz, G. J., Mu, M., Kasibhatla, P. S.,  
20 Morton, D. C., DeFries, R. S., Jin, Y., and van Leeuwen, T. T.: Global fire emissions and the  
21 contribution of deforestation, savanna, forest, agricultural, and peat fires (1997–2009), *Atmos.*  
22 *Chem. Phys.*, 10, 11707–11735, doi:10.5194/acp-10-11707-2010, 2010.

23 Whitaker, J. S., and Hamill, T. M.: Ensemble Data Assimilation without Perturbed  
24 Observations, *Mon. Wea. Rev.*, 130, 1913-1924, 2002.

25 Winderlich, J., Chen, H., Gerbig, C., Seifert, T., Kolle, O., Lavrič, Kaier, C., Höfer, A., and  
26 Heimann, H.: Continuous low-maintenance  $\text{CO}_2/\text{CH}_4/\text{H}_2\text{O}$  measurements at the Zotino Tall  
27 Tower Observatory (ZOTTO) in Central Siberia, *Atmos. Meas. Tech.*, 3, 1113-1128,  
28 doi:10.5194/amt-3-1113-2010, 2010.

29 Zhang, H. F., Chen, B. Z., van der Laan-Luijkx, I. T., Chen, J., Xu, G., Yan, J. W., Zhou, L.  
30 X., Fukuyama, Y., Tans, P. P., and Peters, W.: Net terrestrial  $\text{CO}_2$  exchange over China

1 during 2001–2010 estimated with an ensemble data assimilation system for atmospheric CO<sub>2</sub>.  
2 J. Geophys. Res. Atmos., 119, 2013JD021297, doi:10.1002/2013JD021297, 2014a.  
3 Zhang, H. F, Chen, B. Z., van der Laan-Luijkx, Machida, T., Matsueda, H., Sawa, Y,  
4 Fukuyama, Y., Labuschagne, C., Langenfelds, R., van der Schoot, M., Xu, G., Yan, J. W.,  
5 Zhou, L. X., Tans, P. P., and Peters, W.: Estimating Asian terrestrial carbon fluxes from  
6 CONTRAIL aircraft and surface CO<sub>2</sub> observations for the period 2006 to 2010, Atmos. Chem.  
7 Phys., 14, 5807-5824, doi:10.5194/acp-14-7807-2014, 2014b.  
8

1 Table 1. Information on observation sites located in the Asia and Europe region. MDM  
 2 represents the model-data mismatch which is the observation error.

Site	Location	Latitude	Longitude	Height (Sampling height) (m)	Laboratory (Cooperating agency)	MDM (ppm)
AZV	Azovo, Russia	54.71°N	73.03°E	110(50)	NIES	3
BRZ	Berezorechka, Russia	56.15°N	84.33°E	168(80)	NIES	3
DEM	Demyanskoe, Russia	59.79°N	70.87°E	63(63)	NIES	3
IGR	Igrim, Russia	63.19°N	64.41°E	9(47)	NIES	3
KRS	Karasevoe, Russia	58.25°N	82.42°E	76(67)	NIES	3
NOY	Noyabrsk, Russia	63.43°N	75.78°E	108(43)	NIES	3
SVV	Savvushka, Russia	51.33°N	82.13°E	495(52)	NIES	3
VGN	Vaganovo, Russia	54.50°N	62.32°E	192(85)	NIES	3
YAK	Yakutsk, Russia	62.09°N	129.36°E	264(77)	NIES	3
WLG	Mt. Waliguan, China	36.29°N	100.9°E	3810	CMA/ESRL	1.5
BKT	Bukit Kototabang, Indonesia	0.20°S	100.32°E	864	ESRL	7.5
WIS	Sede Boker, Israel,	31.13°N	34.88°E	400	ESRL	2.5
KZD	Sary Taukum, Kazakhstan	44.45°N	77.57°E	412	ESRL	2.5
KZM	Plateau Assy, Kazakhstan	43.25°N	77.88°E	2519	ESRL	2.5
TAP	Tae-ahn Peninsula, South Korea	36.73°N	126.13°E	20	ESRL	5
UUM	Ulaan Uul, Mongolia	44.45°N	111.10°E	914	ESRL	2.5
CRI	Cape Rama, India	15.08°N	73.83°E	60	CSIRO	3
LLN	Lulin, Taiwan	23.47°N	120.87°E	2862	ESRL	7.5
SDZ	Shangdianzi, China	40.39°N	117.07°E	287	CMA/ESRL	3
MNM	Minamitorishima, Japan	24.29°N	153.98°E	8	JMA	3
RYO	Ryori, Japan	39.03°N	141.82°E	260	JMA	3
YON	Yonagunijima, Japan	24.47°N	123.02°E	30	JMA	3
GSN	Gosan, South Korea	33.15°N	126.12°E	72	NIER	3
BAL	Baltic Sea, Poland	55.35°N	17.22°E	3	ESRL (MIR*)	7.5
BSC	Black Sea, Constanta, Romania	44.17°N	28.68°E	3	ESRL (RMRI*)	7.5
HUN	Hegyhatsal, Hungary	46.95°N	16.65°E	248	ESRL (HMS*)	7.5
OBN	Obninsk, Russia	55.11°N	36.60°E	183	ESRL	7.5
OXK	Ochsenkopf, Germany	50.03°N	11.80°E	1022	ESRL (MPI-BGC*)	2,5
PAL	Pallas-Sammaltunturi, GaW Station, Finland	67.97°N	24.12°E	560	ESRL (FMI*)	2.5
STM	Ocean Station M, Norway	66.00°N	2.00°E	0	ESRL (MET Norway*)	1.5

3 \*Cooperating agencies of observation sites in Europe: Morski Instytut Rybacki (MIR), Romanian Marine  
 4 Research Institute (RMRI), Hungarian Meteorological Service (HMS), Max Planck Institute for  
 5 Biogeochemistry (MPI-BGC), Finnish Meteorological Institute (FMI), Norwegian Meteorological Institute  
 6 (MET Norway).

1 Table 2. A prior and optimized surface CO<sub>2</sub> fluxes and their one-sigma uncertainties (Pg C  
 2 yr<sup>-1</sup> Region<sup>-1</sup>) of global total, land, ocean, and other regions averaged spatially from 2002 to  
 3 2009.

Region	A priori	CNTL	JR.
Eurasian Boreal	-0.07±1.10	-1.17±0.93	-0.77±0.70
Eurasian Temperate	-0.05±0.49	-0.31±0.41	-0.36±0.40
Europe	-0.01±-0.76	-0.20±0.67	-0.37±0.64
North American Boreal	-0.04±0.61	-0.30±0.38	-0.36±0.38
North American Temperate	-0.02±0.66	-0.55±0.41	-0.59±0.41
Northern Hemisphere total	-1.42±1.85	-3.21±1.49	-3.21±1.34
Tropical total	0.06±0.80	0.12±0.74	0.11±0.74
Southern Hemisphere total	-2.57±0.97	-2.46±0.81	-2.45±0.81
Global total	-3.94±2.24	-5.54±1.85	-5.55±1.72
Global land	-1.33±1.90	-3.59±1.57	-3.52±1.43
Global ocean	-2.61±1.19	-1.95±0.97	-2.03±0.96

1 Table 3. The optimized surface CO<sub>2</sub> fluxes (Pg C yr<sup>-1</sup> Region<sup>-1</sup>) of ecosystem types at Eurasian Boreal, Eurasian Temperate, Europe, North  
 2 American Boreal, and North American Temperate region averaged over 2002 - 2009.

Ecosystem type	Eurasian Boreal		Eurasian Temperate		Europe		North American Boreal		North American Temperate	
	CNTL	JR	CNTL	JR	CNTL	JR	CNTL	JR	CNTL	JR
Conifer Forest	-0.815	-0.337	-0.005	-0.005	-0.067	-0.069	-0.107	-0.121	-0.054	-0.069
Broadleaf Forest	-0.006	-0.013	-0.004	-0.005	-0.005	-0.005	0.000	0.000	-0.002	-0.002
Mixed Forest	-0.049	-0.090	-0.029	-0.034	-0.025	-0.063	-0.053	-0.054	-0.019	-0.021
Grass/Shrub	-0.035	-0.056	-0.247	-0.285	-0.016	-0.032	0.000	-0.001	-0.077	-0.081
Tropical Forest	0.000	0.000	-0.001	-0.001	0.000	0.000	0.000	0.000	0.000	0.000
Scrub/Woods	0.000	0.000	-0.002	-0.002	-0.001	-0.001	0.000	0.000	-0.013	-0.013
Semitundra	-0.145	-0.188	-0.007	-0.009	-0.008	-0.009	-0.057	-0.086	-0.010	-0.011
Fields/Woods/Savanna	-0.012	-0.021	-0.005	-0.005	0.003	-0.009	-0.004	-0.004	-0.149	-0.153
Northern Taiga	-0.094	-0.029	0.000	0.000	-0.006	-0.007	-0.066	-0.077	0.000	0.000
Forest/Field	-0.003	-0.008	0.006	0.006	-0.086	-0.105	-0.001	-0.001	-0.012	-0.016
Wetland	-0.002	-0.014	0.000	-0.000	-0.001	-0.002	-0.003	-0.006	-0.002	-0.003
Shrub/Tree/Suc	0.000	0.000	-0.001	-0.001	0.000	0.000	0.000	0.000	0.000	0.000
Crops	-0.002	-0.008	-0.019	-0.022	-0.007	-0.075	0.000	0.000	-0.216	-0.227
Wooded tundra	-0.003	-0.005	0.000	0.000	0.003	0.003	-0.003	-0.002	0.000	0.000
Water	0.000	0.000	0.000	0.000	0.000	0.000	-0.001	-0.001	-0.001	-0.001

1 Table 4. Average differences between model CO<sub>2</sub> concentrations (ppm) simulated using the  
2 background and the observed CO<sub>2</sub> concentration (ppm) (fourth and sixth columns), model  
3 CO<sub>2</sub> concentrations (ppm) simulated using the optimized surface CO<sub>2</sub> flux and the observed  
4 CO<sub>2</sub> concentration (ppm) (fifth and seventh columns), and average innovation  $\chi^2$  from 2002 to  
5 2009 at observation sites located in Asia and Europe (eighth column).

Region	Site	MDM [ppm]	CNTL		JR		Innovation $\chi^2$
			Bias (background)	Bias (optimized)	Bias (background)	Bias (optimized)	
Eurasian	AZV	3	1.68	1.04	0.77	0.19	0.85
Boreal	BRZ	3	1.41	0.68	0.67	0.39	1.17
	DEM	3	0.15	-0.84	0.32	0.11	0.84
	IGR	3	-1.58	-2.71	-0.52	-1.26	1.15
	KRS	3	0.57	-0.22	0.27	0.12	1.22
	NOY	3	-0.02	-1.06	0.16	0.00	0.86
	SVV	3	1.25	0.71	0.63	0.09	0.96
	VGN	3	2.55	2.11	1.50	0.84	1.18
	YAK	3	0.23	-2.18	0.87	0.03	1.36
Eurasian	WLG	1.5	0.17	0.19	0.15	0.16	1.09
Temperate	BKT	7.5	4.12	4.06	4.13	4.05	0.57
	WIS	2.5	0.27	0.12	0.22	0.07	0.72
	KZD	2.5	1.79	0.98	1.42	1.14	1.26
	KZM	2.5	1.17	0.96	1.13	0.93	1.26
	TAP	5	0.50	0.55	0.58	0.71	0.58
	UUM	2.5	0.24	-0.07	0.20	0.12	1.05
	CRI	3	-1.95	-1.57	-1.94	-1.56	0.66
	LLN	7.5	4.42	3.09	4.42	3.09	0.47
	SDZ	3	-3.02	-5.26	-3.09	-5.28	2.08
	MNM	3	0.56	0.52	0.59	0.56	0.17
	RYO	3	1.26	1.16	1.32	1.32	1.07
	YON	3	1.10	0.98	1.14	1.07	0.56
	GSN	3	-1.92	-1.71	-1.92	-1.70	1.83
Europe	BAL	7.5	-1.23	-1.32	-1.31	-1.45	0.37
	BSC	7.5	-4.12	-4.97	-4.12	-5.13	1.01
	HUN	7.5	0.93	0.53	0.86	0.36	0.46
	OBN	7.5	0.70	-0.71	0.59	-0.89	0.44
	OXK	2.5	0.50	0.02	0.43	-0.09	1.52
	PAL	2.5	0.47	0.07	0.58	0.16	0.76
	STM	1.5	0.54	0.42	0.55	0.42	0.76

6

1 Table 5. Bias, root mean square difference, mean absolute error, and Pearson's Correlation  
 2 Coefficient of the model CO<sub>2</sub> concentration of CNTL and JR experiments in comparison with  
 3 the vertical profile of CO<sub>2</sub> concentrations at BRZ site.

Altitude (km)	Bias (ppm)		Root-Mean-Square Difference (ppm)		Mean Absolute Error (ppm)		Pearson's Correlation Coefficient	
	CNTL	JR	CNTL	JR	CNTL	JR	CNTL	JR
~ 0.5	-0.38±4.73	-0.05±4.39	4.06	3.75	3.42	3.07	0.94	0.95
0.5 ~ 1.0	0.23±4.05	0.42±3.75	3.58	3.33	2.94	2.72	0.94	0.95
1.0 ~ 1.5	0.19±3.80	0.31±3.53	3.35	3.11	2.70	2.49	0.94	0.95
1.5 ~ 2.0	0.22±3.38	0.33±3.19	2.94	2.79	2.33	2.19	0.93	0.94
2.0 ~ 2.5	0.02±3.19	0.08±3.07	2.64	2.54	2.19	2.11	0.93	0.94
2.5 ~ 3.0	0.79±2.84	0.80±2.53	1.44	1.30	2.21	1.99	0.92	0.94
3.0 ~	0.61±3.15	0.61±2.91	1.49	1.38	2.42	2.26	0.89	0.91

4

5



1 Table 6. Optimized surface CO<sub>2</sub> fluxes (Pg C yr<sup>-1</sup>) from this study and other inversion studies.

Citation	Area	Estimate surface CO <sub>2</sub> flux	Period	Remarks
This study	Eurasian Boreal	-0.77±0.70	2002-2009	JR experiment
Saeki et al. (2013)	Eurasian Boreal	-0.35±0.61	2000-2009	Including biomass burning (0.11Pg C yr <sup>-1</sup> ), Using JR-STATION observations
Zhang et al. (2014b)	Eurasian Boreal	-1.02±0.91	2006-2010	Using CONTRAL observations
Maki et al. (2010)	Eurasian Boreal	-1.46±0.41	2001-2007	
Dolman et al. (2012)	Russia <sup>a</sup>	-0.613		Average of inventory-based, eddy covariance, and inversion methods
CT2013B <sup>b</sup>	Eurasian Boreal	-1.00±3.75	2002-2009	
This study	Europe	-0.38±0.64	2002-2009	JR experiment
Reuter et al. (2014)	Europe	-0.75±0.63	2008-2009	
		-1.02±0.30	2010	Using satellite data
CTE2014 <sup>c</sup>	Europe	-0.07±0.49	2002-2009	
		-0.11±0.38	2008-2009	

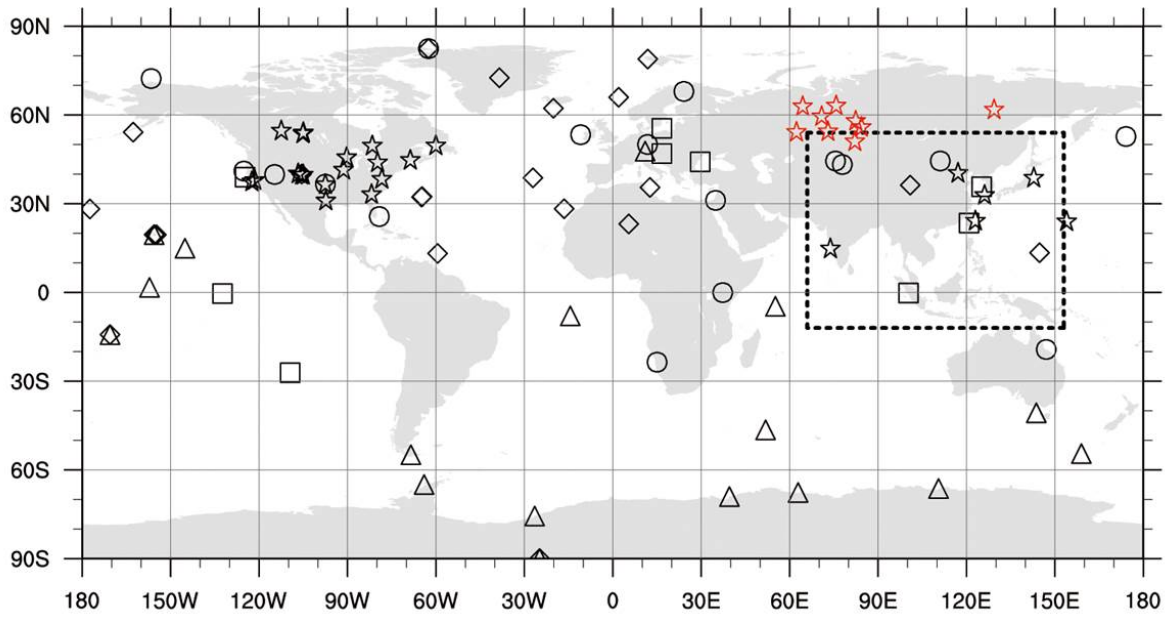
2 <sup>a</sup>Including Ukraine, Belarus and Kazakhstan (total area is  $17.1 \times 10^{12}$  m<sup>2</sup>)

3 <sup>b</sup>The results of CT2013B (<http://www.esrl.noaa.gov/gmd/ccgg/carbontracker/CT2013B/>) were  
4 derived from (<ftp://aftp.cmdl.noaa.gov/products/carbontracker/co2/fluxes/>).

5 <sup>c</sup>The results of CTE2014 (CarbonTracker Europe, Peters et al., 2010) were derived from  
6 (<ftp://ftp.wur.nl/carbontracker/data/fluxes/>).

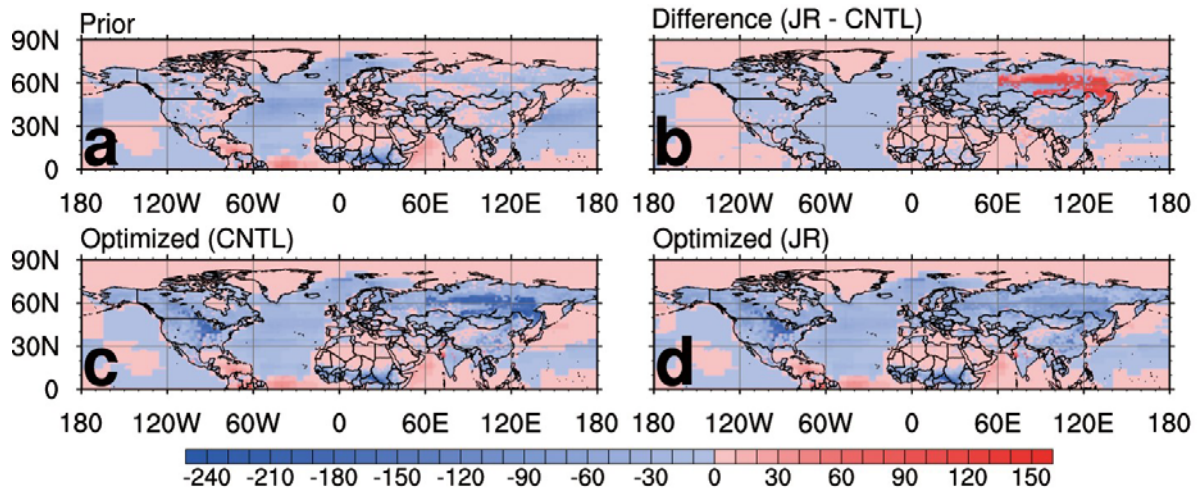
7

8



1  
2  
3  
4  
5  
6  
7

Figure 1. Observation networks of CO<sub>2</sub> concentrations around the globe and the nested domain of the TM5 transport model over Asia (dashed box). Each observation site is assigned to different categories ( $\Delta$ : MBL;  $\circ$ : Continental;  $\diamond$ : Mixed land/ocean and mountain;  $\star$ : Continuous;  $\square$ : Difficult). JR-STATION observation sites are represented in red color.



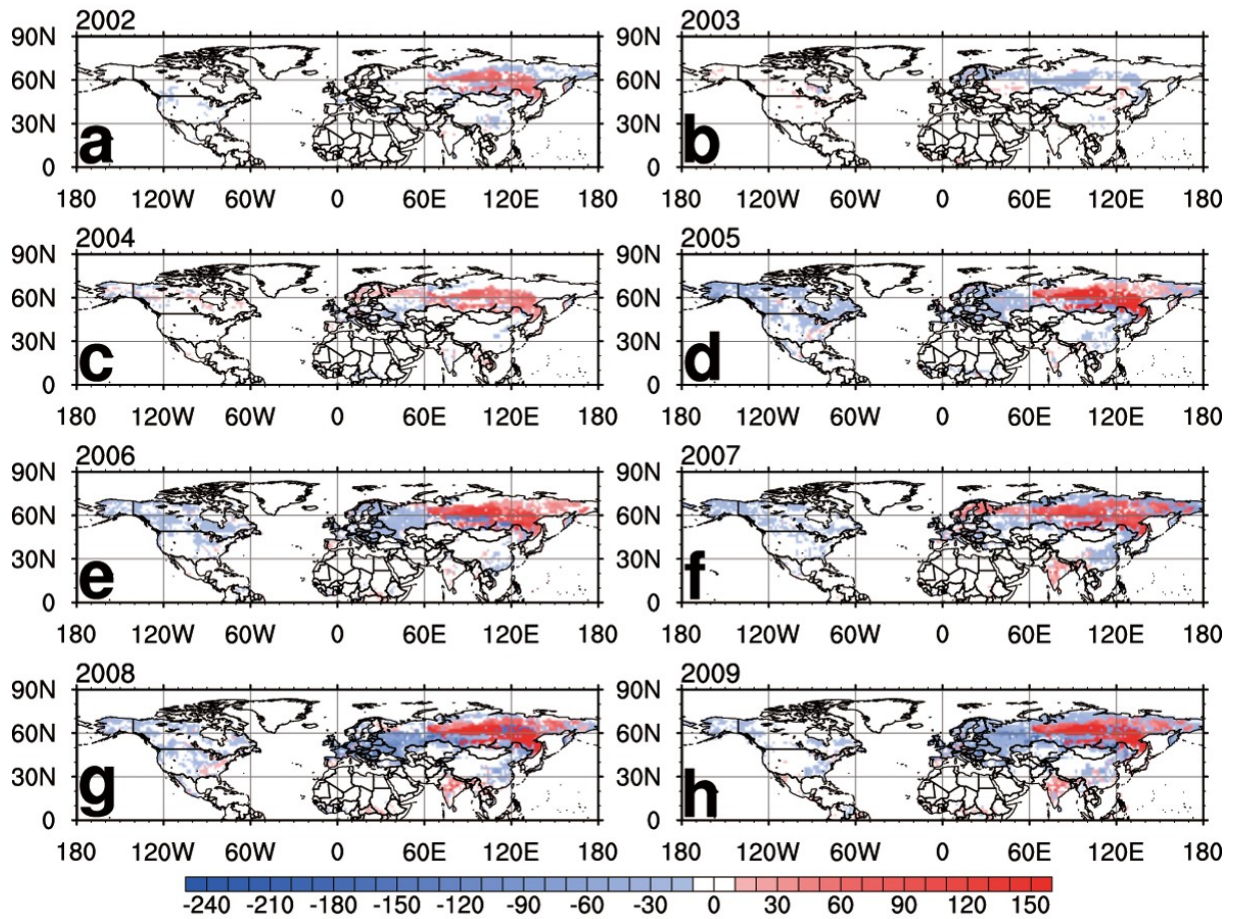
1

2

3 Figure 2. Average biosphere and ocean fluxes ( $\text{gC m}^{-2} \text{yr}^{-1}$ ) from 2002 to 2009 of (a) the prior  
 4 flux, (b) the difference between the optimized fluxes in the JR and CNTL experiments, (c) the  
 5 optimized flux in the CNTL experiment, and (d) the optimized flux in the JR experiment.  
 6 Blue colors (negative) denote net CO<sub>2</sub> flux uptake while red colors (positive) denote net CO<sub>2</sub>  
 7 release to the atmosphere. The difference is calculated by subtracting surface CO<sub>2</sub> flux of  
 8 CNTL experiment from that of JR experiment.

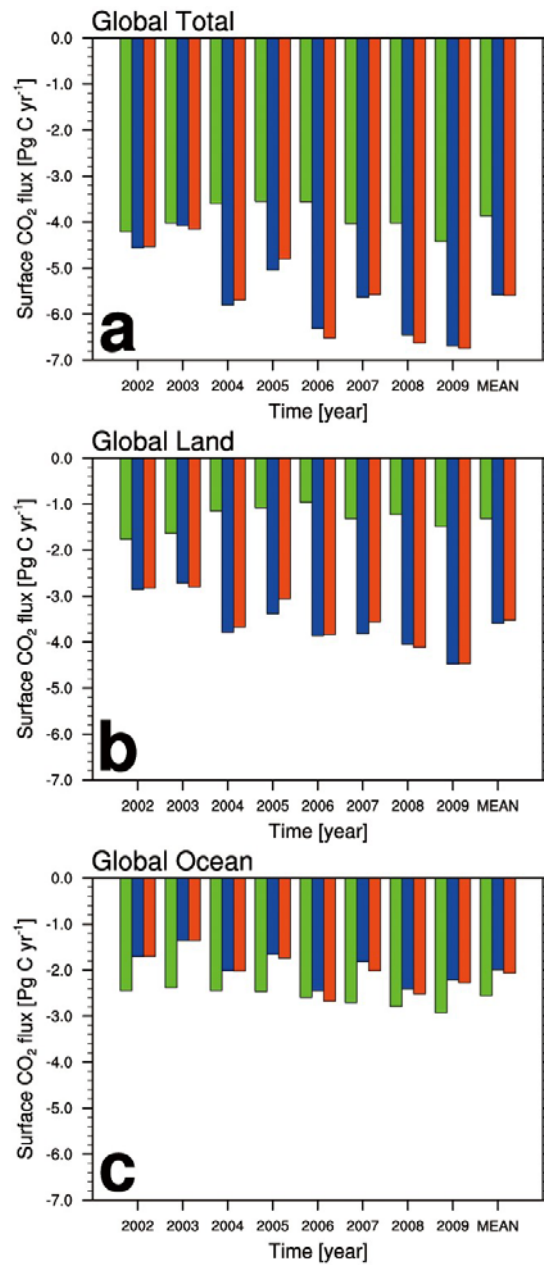
9

10



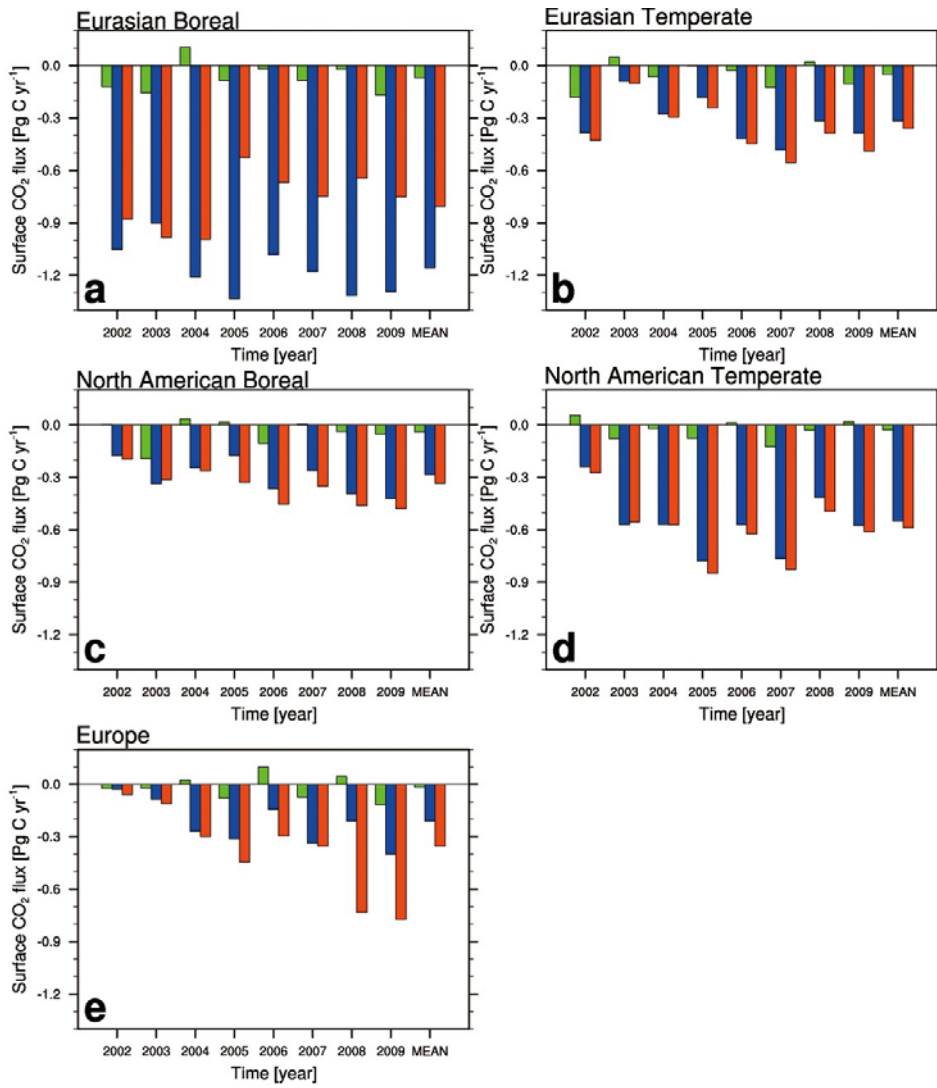
1  
2  
3  
4  
5  
6  
7  
8  
9

Figure 3. The difference between the optimized biosphere fluxes from the JR and CNTL experiment ( $\text{g C m}^{-2} \text{ yr}^{-1}$ ) of (a) 2002, (b) 2003, (c) 2004, (d) 2005, (e) 2006, (f) 2007, (g) 2008, and (h) 2009. Blue colors (negative) denote net CO<sub>2</sub> flux uptake while red colors (positive) denote net CO<sub>2</sub> release to the atmosphere. The difference is calculated by subtracting surface CO<sub>2</sub> flux of CNTL experiment from that of JR experiment.



1  
2  
3  
4  
5  
6

Figure 4. Annual and average biosphere and ocean fluxes (Pg C yr<sup>-1</sup>) from the prior (green bar), CNTL (blue bar) and JR (red bar) experiment aggregated over the (a) whole globe, (b) land, and (c) ocean.



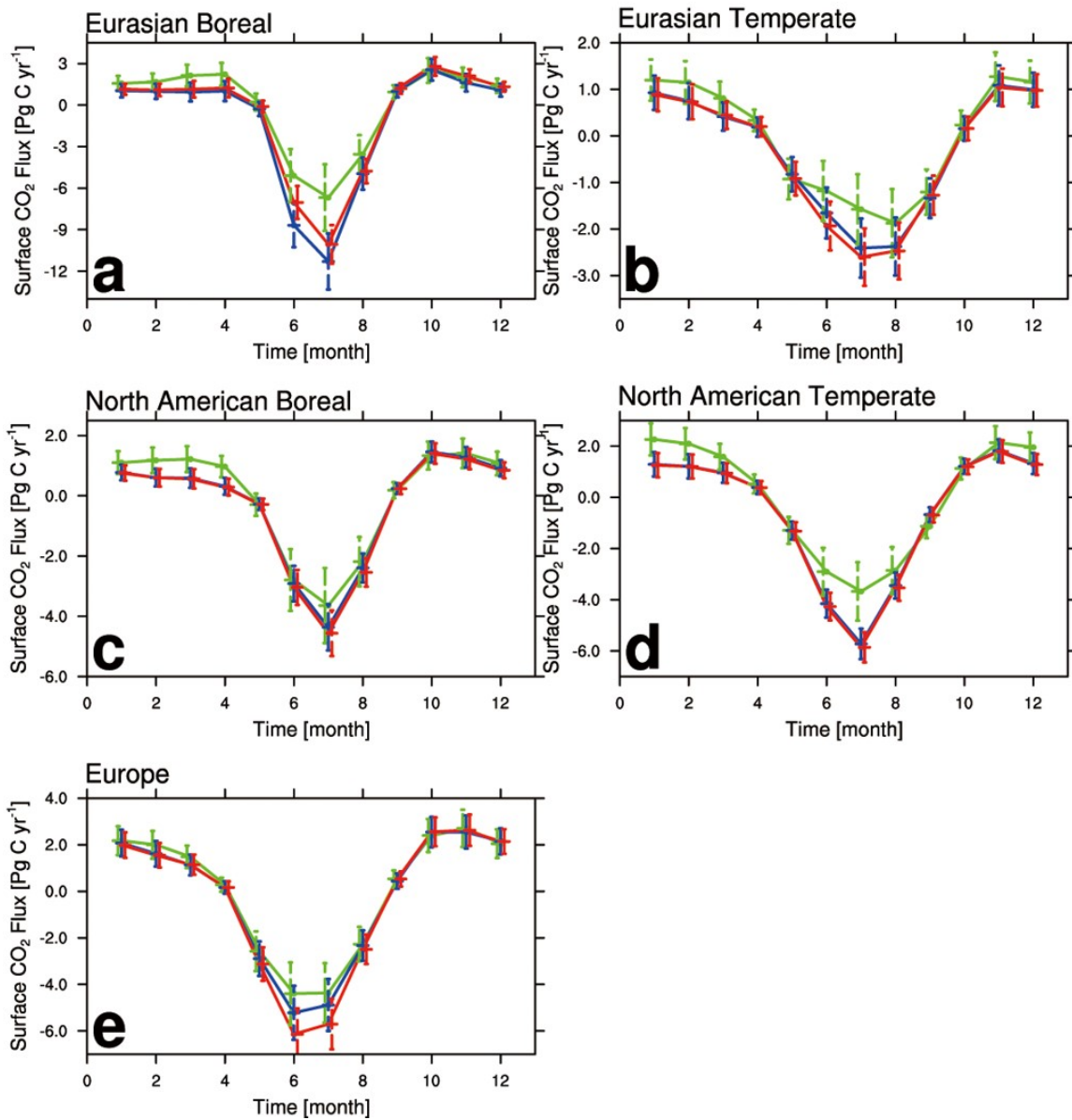
1

2 Figure 5. Annual and average biosphere fluxes (Pg C yr<sup>-1</sup>) from the prior (green bar), CNTL  
 3 (blue bar) and JR (red bar) experiment aggregated over the (a) Eurasian Boreal, (b) Eurasian  
 4 Temperate, (c) North American Boreal, (d) North American Temperate, and (e) Europe.

5

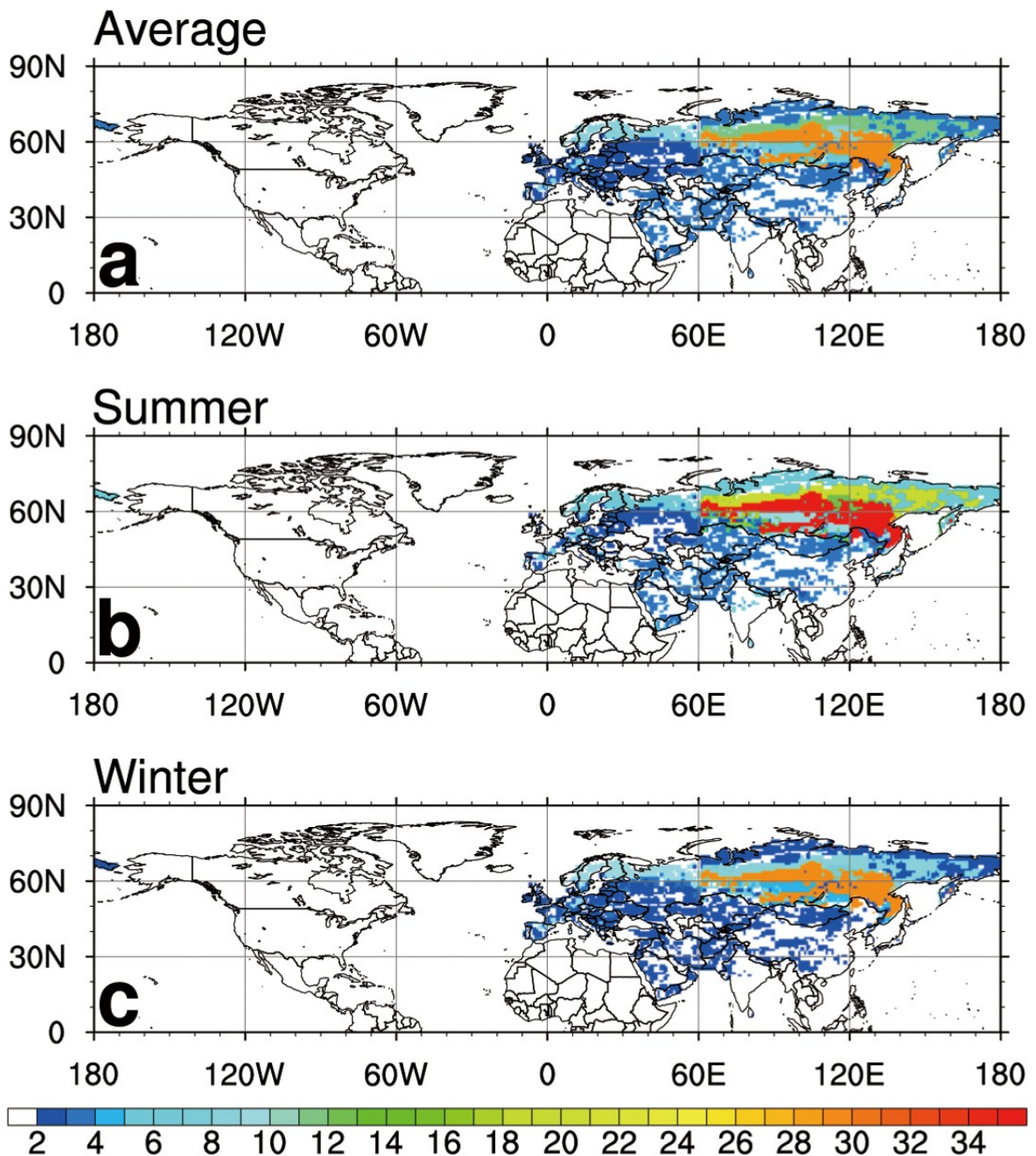
6





1  
2  
3  
4  
5  
6  
7

Figure 6. The monthly prior (green) and optimized biosphere fluxes averaged from 2002 to 2009 of CNTL (blue) and JR (red) experiment with their uncertainties over the (a) Eurasian Boreal, (b) Eurasian Temperate, (c) North American Boreal, (d) North American Temperate, and (e) Europe.



1

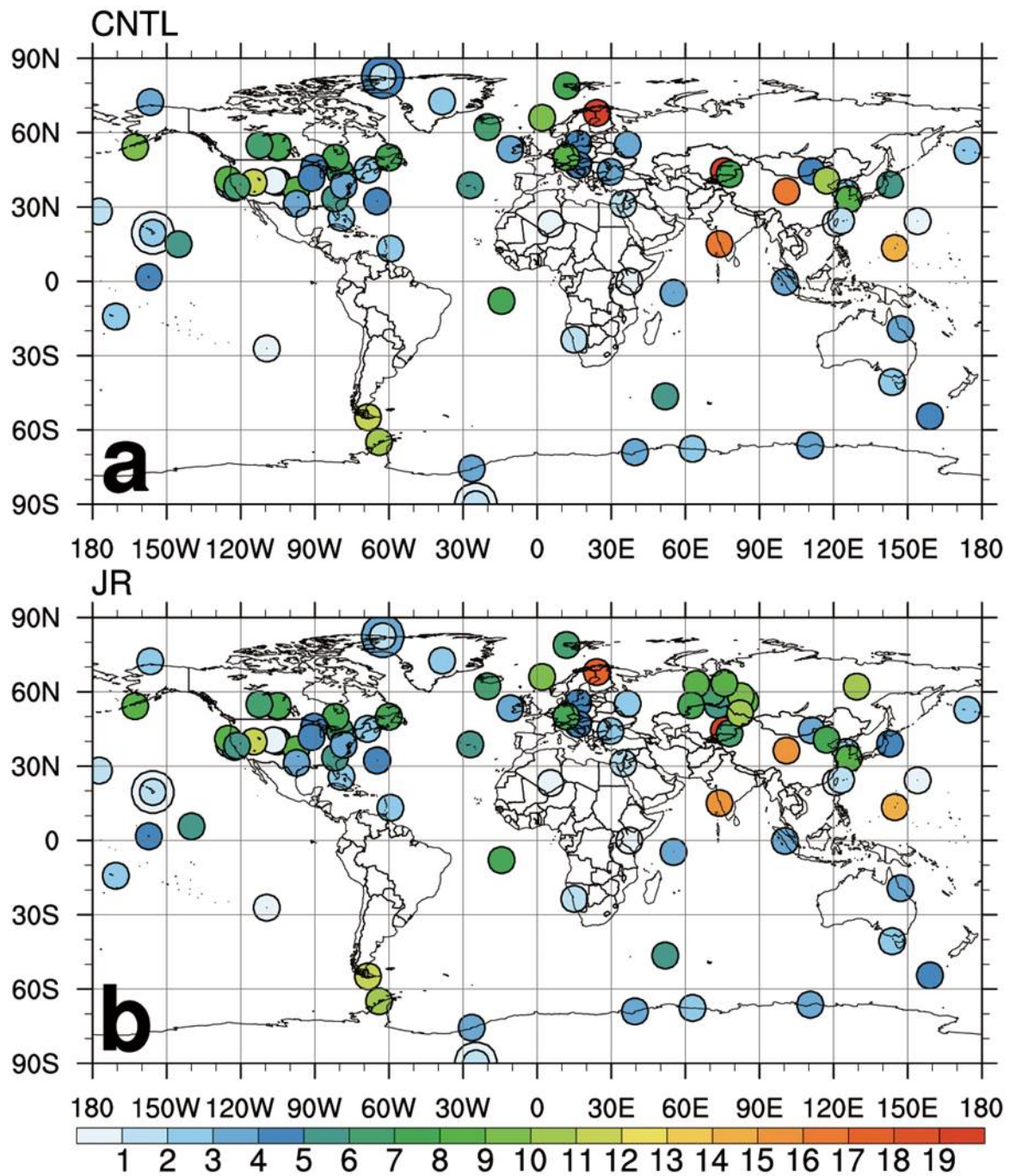
2

3 Figure 7. (a) Average uncertainty reduction (%) from 2002 to 2009, average uncertainty  
 4 reduction (%) in (b) summer, and (c) winter for the estimated uncertainty of the JR  
 5 experiment relative to that of the CNTL experiment. Red (blue) denotes relatively high (low)  
 6 value of uncertainty reduction.

7

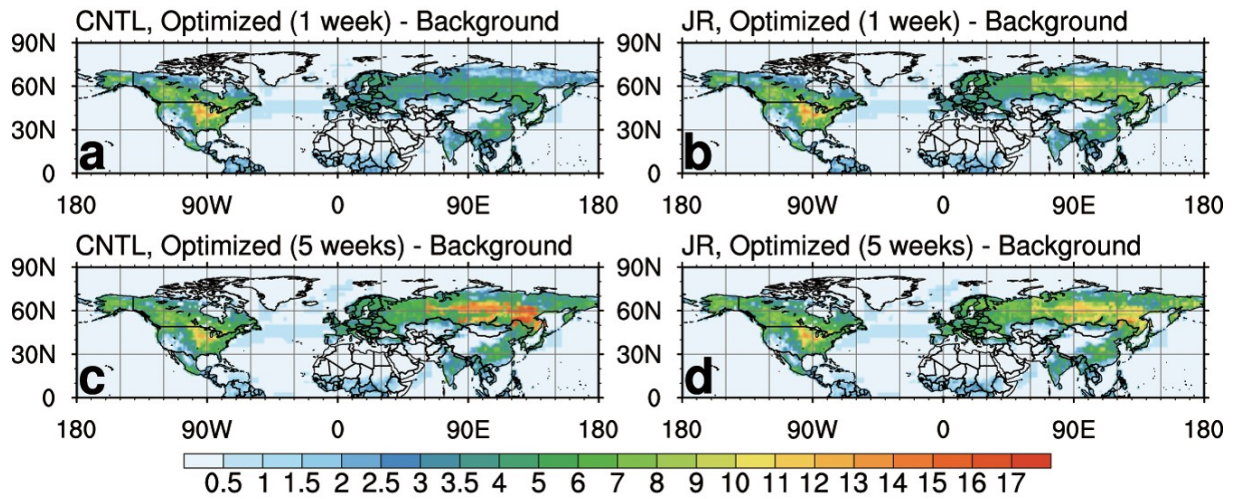
8





1  
2  
3  
4  
5  
6  
7

Figure 8. Self-sensitivity at each observation site averaged from 2002 to 2009 of (a) CNTL experiment and (b) JR experiment. The overlapping observation sites at the same locations or at close locations are distinguished by different sizes of circles. Red (blue) denotes relatively high (low) value of self-sensitivity.



1

2

3 Figure 9. RMSD averaged from 2002 to 2009 between the background flux and posterior flux  
 4 optimized in Northern Hemisphere summer by 1 week of observations of (a) CNTL and (b)  
 5 JR experiment; and by 5 weeks of observations of (c) CNTL and (d) JR experiment. The units  
 6 are g C m<sup>-2</sup> week<sup>-1</sup>. Red (blue) denotes relatively high (low) value of RMSD.